Contrib Mineral Petrol (2006) 151: 582–599
DOI 10.1007/s00410-006-0070-y

ORIGINAL PAPER

James S. Scoates · Mauro Lo Cascio
Dominique Weis · Donald H. Lindsley

Experimental constraints on the origin and evolution of mildly alkalic basalts from the Kerguelen Archipelago, Southeast Indian Ocean

Received: 18 February 2005 / Accepted: 18 January 2006 / Published online: 17 March 2006

Abstract This experimental study examines the role of clinopyroxene fractionation on major element trends and alkalinity variations in mildly alkalic basalts from the Kerguelen Archipelago, Southeast Indian Ocean. Equilibrium crystallization experiments were carried out on a natural basalt (MgO = 5 wt.%, alkalinity index = 0.10) over a range of pressures (0–1.43 GPa) and water contents (nominally dry to hydrous, 1.2 wt.% H_2O) under relatively oxidizing conditions (Δlog FMQ = +1 to +2) at 0 GPa and relatively reducing conditions (Δlog FMQ = 0 to –2) at all higher pressures. The hydrous experiments at 0.93 GPa closely reproduce most of the compositional variations in the 24–25 Ma mildly alkalic lavas from the archipelago, which supports a major role for high-Al clinopyroxene fractionation (5–9 wt.% Al_2O_3) at pressures corresponding to the base of the Northern Kerguelen Plateau (15–20 km). However, clinopyroxene fractionation at depth fails to produce important changes in the alkalinity of the residual melts. The transition from tholeiitic to mildly alkalic basalts on the Kerguelen Archipelago thus reflects primarily changes in melting conditions (lower extents of partial melting at higher pressures), which is related to crustal and lithospheric thickening as distance from the Southeast Indian Ridge increased over time from 43 to 24 Ma.

Communicated by T. L. Grove

J. S. Scoates (✉) · M. Lo Cascio · D. Weis
Department of Earth & Environmental Sciences (DSTE),
Université Libre de Bruxelles CP160/02,
Avenue F.D. Roosevelt 50, Brussels, Belgium
E-mail: jscoates@eos.ubc.ca
Tel.: +1-604-8223667
Fax: +1-604-8226088

D. H. Lindsley
Department of Geosciences,
State University of New York at Stony Brook,
Stony Brook, NY, USA

Present address: J. S. Scoates
Department of Earth & Ocean Sciences,
University of British Columbia, 6339 Stores Road,
Vancouver, Canada

Present address: M. Lo Cascio
Department of Geological Sciences,
Brown University, 324 Brook St – Box 1846,
Providence, RI, USA

Present address: D. Weis
Department of Earth & Ocean Sciences,
University of British Columbia, 6339 Stores Road,
Vancouver, Canada

Introduction

Many oceanic islands contain individual volcanoes or volcanic sequences that record the transition from tholeiitic to alkalic basalts (e.g., Hawaii, Frey et al. 1990, Lipman et al. 2000; Galápagos, McBirney and Williams 1969, Geist et al. 1986, Naumann and Geist 1999; Iceland, Furman et al. 1991; Réunion, Albarède et al. 1997; Kerguelen, Frey et al. 2002). Hawaiian volcanoes typically evolve from an early submarine alkalic stage through a tholeiitic shield-building stage, and finally to a post-shield alkalic stage as the individual volcanoes on the northwest-moving Pacific Plate pass over the Hawaiian hotspot. These changes in alkalinity are consistent with changes in the degrees and depths of partial melting of a common mantle source, where alkalic basalts reflect lower degrees of melting at higher pressures relative to tholeiitic basalts (Chen and Frey 1983). Partial melting of silica-deficient garnet pyroxenite could also be responsible for producing strongly nepheline-normative compositions (Hirschmann et al. 2003), although this process may only play a minor role in controlling the major element trends of ocean island basalts (Keshav et al. 2004). In contrast, contemporaneous alkalic and tholeiitic basalts from the Cerro Azul volcano on the Galápagos Archipelago appear to be related primarily by fractional crystallization of clinopyroxene-rich assemblages in the lower oceanic crust and mantle and do not

require either different degrees of melting or different source rocks (Naumann and Geist 1999; Naumann et al. 2002). Fractionation of an olivine-clinopyroxene assemblage at lithospheric mantle pressures is also responsible for driving tholeiitic basalts from Piton de la Fournaise volcano on Réunion into the field of alkalic basalts (Albarède et al. 1997). Indeed, extensive high-pressure clinopyroxene fractionation in the parent magmas to ocean island basalts is consistent with geochemical trends from a wide range of oceanic islands (e.g., Albarède 1992), thus the differentiation of tholeiitic magmas at high pressure may be a viable mechanism for producing alkalic basalts under the appropriate conditions.

In this paper, we examine the role of clinopyroxene fractionation on major element trends in tholeiitic to mildly alkalic basalts from the 6,500 km^2 Kerguelen Archipelago based on a series of equilibrium crystallization experiments on a natural basalt at dry and slightly hydrous (1.2 wt.% H_2O) conditions and at relatively high (0.4–1.4 GPa) and low (<0.1 MPa) pressures. The Kerguelen Archipelago, the largest oceanic island after Hawaii and Iceland, is the emergent part of the 19–20 km thick Northern Kerguelen Plateau, which is located on the nearly stationary Antarctic Plate in the Southeast Indian Ocean (Fig. 1). The Northern Kerguelen Plateau began to form at ~40 Ma (e.g., Weis and Frey 2002), when the Southeast Indian Ridge and the Kerguelen hotspot were coincident, and since 40 Ma the ridge has moved to the north relative to the plateau. The alkalinity of lavas erupted on the Northern Kerguelen Plateau and Kerguelen Archipelago has increased as the distance between the ridge and the plume has lengthened. Lava compositions range from tholeiitic at Site 1140 (34 Ma) on the northern edge of the Northern Kerguelen Plateau (Weis and Frey 2002), to transitional for the 26–29 Ma flood basalts on the archipelago (Yang et al. 1998; Nicolaysen et al. 2000; Frey et al. 2000a, 2002; Doucet et al. 2002), to mildly alkalic for the youngest (24–25 Ma) lava sequences on the archipelago (Weis et al. 1993; Nicolaysen et al. 2000; Frey et al. 2000a) (Fig. 2). Strongly alkalic, nepheline-normative basanites to phonolites on the archipelago are much younger (6–10 Ma) and occur as minor flows, intrusions, and plugs that crystallized from relatively hydrous, oxidized alkalic parent magmas (Weis et al. 1993; Freise et al. 2003). Importantly, petrologic, geobarometric and geochemical results from mildly alkalic lavas of the 24 Ma Mont Crozier section on the Kerguelen Archipelago indicate a significant role for high-pressure fractionation of high-Al clinopyroxene, in the region of the seismic crust-to-mantle transition zone (14–16 km depth) under the archipelago, that is not evident in the older tholeiitic-transitional basalts (Damasceno et al. 2002). The experiments carried out on a sample from the Crozier section in this study demonstrate that crystallization of a clinopyroxene-dominant assemblage at relatively high pressures (0.9 GPa) and slightly hydrous conditions (1.2 wt.% H_2O) is capable of producing most of the characteristic major element geochemical trends of the mildly alkalic lavas (i.e., increasing Al_2O_3 with decreasing MgO). Associated increases in alkalinity, however, are much smaller than the range shown for the mildly alkalic basalts from the Kerguelen Archipelago. Significant changes in alkalinity are thus likely related to the combined effect of clinopyroxene fractionation and a decrease in the extent of melting combined with a decrease in magma supply and an increase in the depth of melting (Weis et al. 1998a; Frey et al. 2000a). These changes are ultimately controlled by crustal and lithospheric thicknesses as the Kerguelen Archipelago and Northern Kerguelen Plateau moved from a ridge-centered position at ~40 Ma to an intraplate setting by 25 Ma.

Characterization of starting material

The starting material (sample OB93-147) for this study is a natural basalt from the Mont Crozier section on the Kerguelen Archipelago (Table 1; Fig. 1b) (Damasceno 1996). Mont Crozier is the highest point (948 m) on the Courbet Peninsula in the eastern part of the Kerguelen Archipelago and represents the thickest stratigraphic section available. Detailed sampling of the nearly 1,000-meter section in 1993, from Lac Superieur at the base to the summit, yielded 95 whole rock samples. Based primarily on the absence of alteration (or minimal alteration), 44 samples were selected for detailed petrographic observations and combined major and trace element analyses, from which a subset of 25 samples were selected for Sr-Nd-Pb-Hf isotopic analyses. The eruptive age of basalts from the Crozier section is constrained by $^{40}Ar/^{39}Ar$ dating of whole rocks from the base (24.82 ± 0.19 Ma) and top (24.53 ± 0.67 Ma) of the section (Nicolaysen et al. 2000). Damasceno (1996), Damasceno de Oliveira et al. (1997) and Damasceno et al. (1997) presented preliminary geochemical results on the Crozier section. Ion microprobe analyses of clinopyroxene phenocrysts throughout the section were reported by Damasceno et al. (2000), and Hf-Nd isotopic compositions for 11 whole rock samples were published by Mattielli et al. (2002). Damesceno et al. (2002) published a detailed study of plagioclase, clinopyroxene, and olivine phenocryst compositional variation on 15 samples from the Crozier section and outlined a polybaric fractionation history with high-Al clinopyroxene as the major fractionating phase at depth (>0.5 GPa) and plagioclase phenocryst crystallization in shallow-level magma reservoirs prior to eruption.

The majority of the Crozier flows are evolved, low-MgO (<6 wt.%), mildly alkalic basalts to trachybasalts with alkalinity indices (AI = total alkalis $-$ ($SiO_2 \times 0.37 - 14.43$); Rhodes 1996) varying from 0–3.2, from the alkalic-tholeiitic dividing line to well within the alkalic field. Based on their Sr-Nd-Pb-Hf isotopic compositions, Weis et al. (1998b), Mattielli et al. (2002) and Weis et al. (2002) proposed that the isotopic compositions of the Crozier lavas reflect the purest expression of the enriched component of the Kerguelen mantle plume.

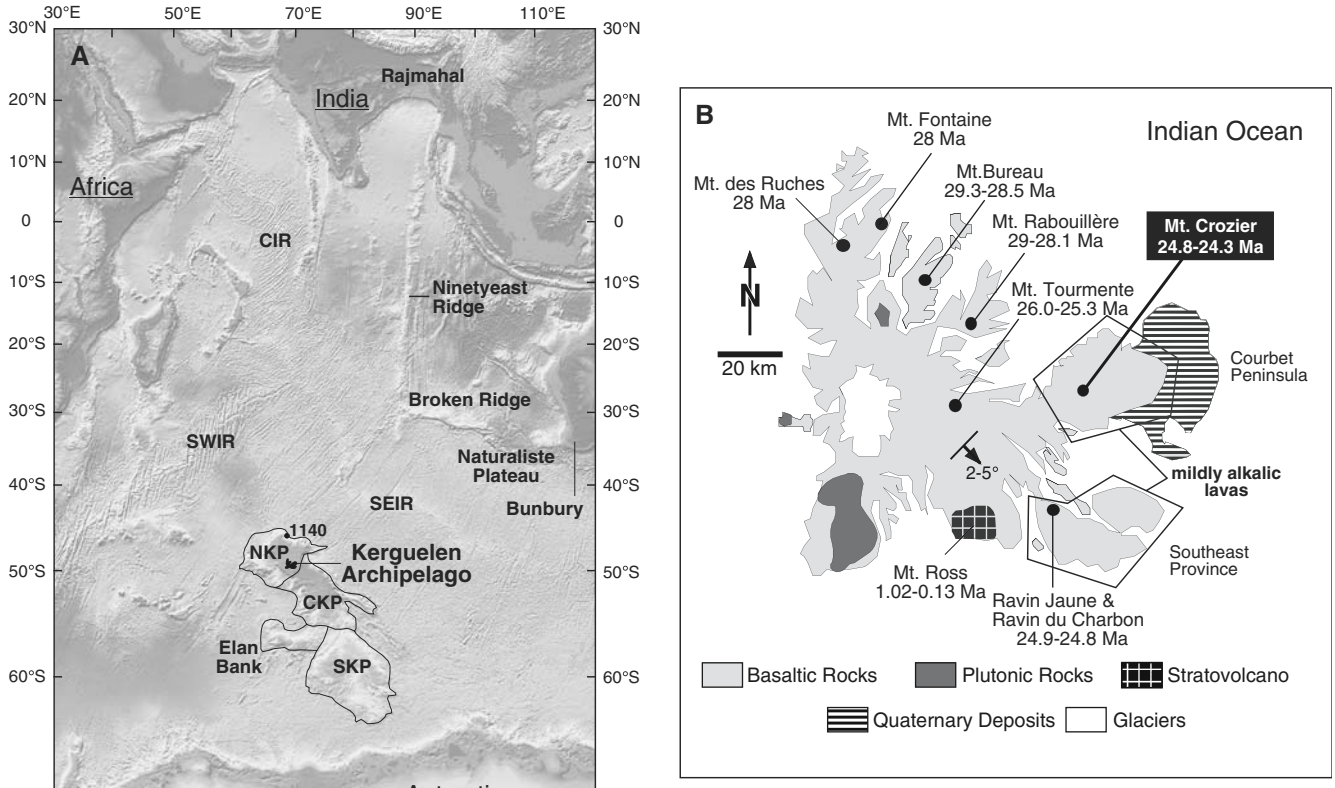

Fig. 1 **a** Bathymetric map of the Indian Ocean from Smith and Sandwell (1997) showing the location of the Kerguelen Archipelago, volcanic structures of the Kerguelen large igneous province, and mid-ocean ridge segments of the Indian Ocean basin. The Kerguelen Plateau is outlined. *NKP* Northern Kerguelen Plateau, *CKP* Central Kerguelen Plateau, *SKP* Southern Kerguelen Plateau, *1140* ODP Leg 183 Site 1140, *SEIR* Southeast Indian Ridge, *SWIR* Southwest Indian Ridge, *CIR* Central Indian Ridge. **b** Simplified geologic map of the Kerguelen Archipelago after Nougier (1970) showing the location of the Mont Crozier basaltic section on the Courbet Peninsula. The starting composition (OB93-147) for this study was sampled at 670 m altitude and is part of volcanic unit C of Damasceno et al. (2002). Also indicated are the basaltic sections for which geochemical data are available: Mt. Bureau and Rabouillère (Yang et al. 1998), Ravin Jaune and Ravin du Charbon from the Southeast Province (Frey et al. 2000a), Mt. des Ruches and Fontaine (Doucet et al. 2002), Mt. Tourmente (Frey et al. 2002), and Mt. Crozier (Damasceno, 1996; Mattielli et al. 2002). $^{40}Ar/^{39}Ar$ ages are reported in Nicolaysen et al. (2000), Frey et al. (2000a), and Doucet et al. (2002). The areas where the 24–25 Ma mildly alkalic lava sequences occur are outlined. Mt. Ross is a young (< 2 Ma) stratovolcano composed of trachybasalts and trachytes (Weis et al. 1998a)

The criteria for selecting sample OB93–147 as the starting material for this study were the following: (1) minor alteration of the sample, which is restricted to local patchy oxidation of the groundmass, (2) phenocrysts are small (> 2 mm length) and volumetrically minor (2.7% plagioclase, 0.3% clinopyroxene, 0.7% olivine) (Damasceno et al. 2002), (3) the MgO content of OB93-147 (5.08 wt.%) is among the highest values for samples from the Crozier section, and (4) the alkalinity index of OB93-147 is 0.10, essentially on the tholeiitic-alkalic boundary, and is the lowest AI of a sample from the Crozier section that is not altered (e.g., K-loss) and shares the trace element and isotopic characteristics of the majority of the sampled flows. At ~5 wt.% MgO, sample OB93-147 clearly represents a fractionated basalt with prior crustal processing (i.e., OB93-147 does not represent a primitive magma composition). The importance of using this particular sample is that it allowed us to test the extent to which crystal fractionation could explain the large alkalinity variations from a single volcanic section on the Kerguelen Archipelago, starting with a sample that combines the lowest AI and highest MgO content from the section.

Experimental and analytical techniques

Experimental procedures

All of the experiments were carried out in the experimental laboratory of D.H. Lindsley at the State University of New York at Stony Brook. The starting composition OB93-147 was initially ground to a powder for whole rock geochemical and isotopic analyses in an agate planetary mill. An aliquot of this material was further ground under ethanol in an agate mortar for 2 h and this powder was used for all of the experiments. Low-pressure experiments were performed in a

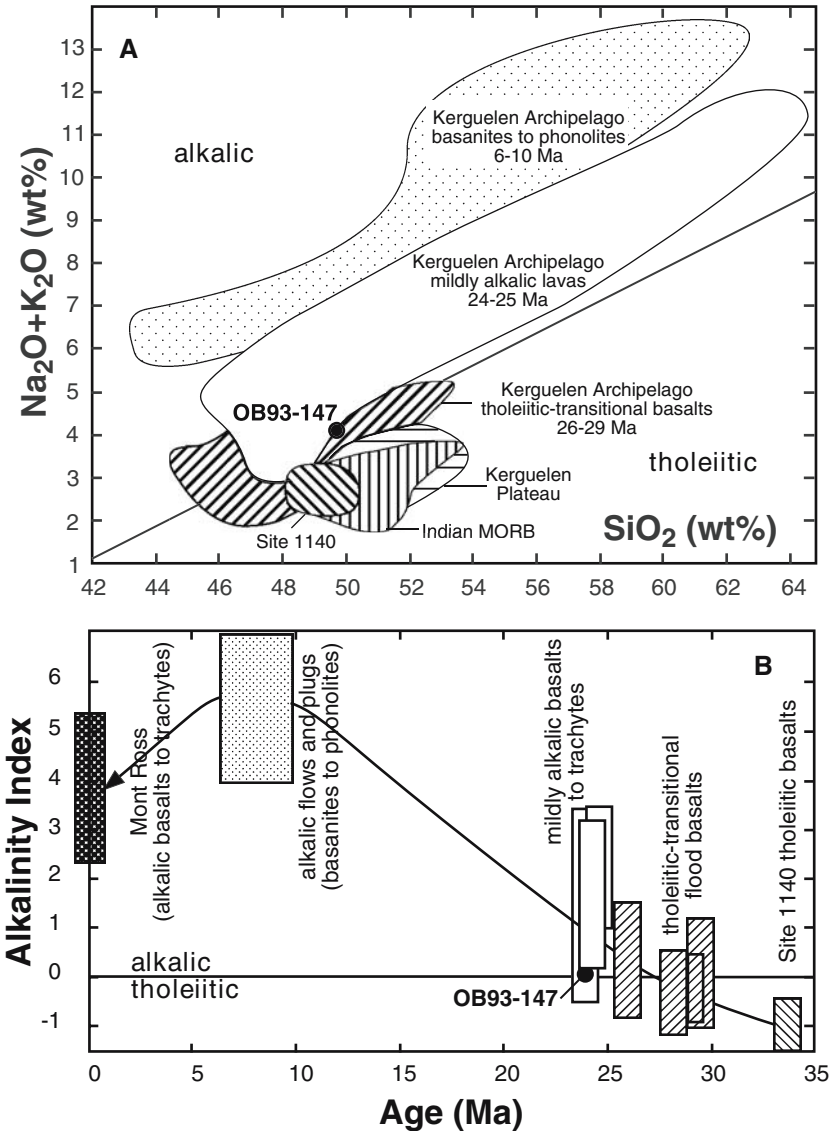

Fig. 2 **a** Diagram of $Na_2O + K_2O$ versus SiO_2 showing the starting composition for this study (OB93-147) along the tholeiitic-alkalic boundary from MacDonald and Katsura (1964) and fields encompassing the different groups of volcanic rocks discussed in this paper. Data sources for the Kerguelen Archipelago lavas (24–25 Ma mildly alkalic lavas and 26–29 Ma tholeiitic-transitional lavas) are indicated in the caption to Fig. 1b. Data sources for remaining chemistry are as follows: ODP Leg 183 Site 1140 on the Northern Kerguelen Plateau (Weis and Frey 2002), Kerguelen Plateau (Mahoney et al. 1995; Frey et al. 2000b), and Indian MORB (Mahoney et al. 1992). For comparison, the field of 6–10 Ma basanites to phonolites from the Upper Miocene Series of the Kerguelen Archipelago is shown (Weis et al. 1993). **b** Diagram of age versus alkalinity index from 35 Ma to the present showing the evolution with time of alkalinity for tholeiitic basalts recovered at ODP Leg 183 Site 1140 through the 26–29 Ma transitional-tholeiitic basalts and 24–25 Ma mildly alkalic basalts on the Kerguelen Archipelago. The alkalinity index reflects the distance of a sample from the tholeiitic-alkalic boundary of MacDonald and Katsura (1964) as shown in Fig. 2a and is defined in the text

Pt-wound quench furnace. The powdered sample was placed in a crimped $Au_{80}Pd_{20}$ tube, which in turn was placed in a silica glass tube. The silica tube was evacuated and the sample dried at 800°C for 20 min in the presence of an Fe oxygen getter. As the pressure inside the silica tube is much lower than 1 atm, we will refer to this set of experiments as "0 GPa" runs. The silica tube was sealed, hung by a Pt wire in the furnace, and gradually lowered to the hot spot. At the end of the run, the sample was quenched in cold water. The combined thermal gradient and thermocouple uncertainty is probably less than 5°C. The estimated oxygen fugacity (f_{O2}) for these runs probably varied between 1 and 2 log units above FMQ based on experiments made with the same set-up having similar starting materials (Nekvasil et al. 2004) and were calculated using the QUILF method of Andersen et al. (1993).

High-pressure experiments were conducted in a piston cylinder apparatus up to 1.43 GPa using graphite capsules. Extra-dense $BaCO_3$ sleeves with exterior Pb

Table 1 Composition of the starting material (in wt.% oxides) determined by XRF

Sample	SiO_2	TiO_2	Al_2O_3	Fe_2O_3	MnO	MgO	CaO	Na_2O	K_2O	P_2O_5	Total	Mg#[a]	AI[b]
OB93–147	49.11	2.72	14.90	13.43	0.19	5.08	10.48	2.88	0.96	0.34	100.09	0.40	0.10

Major element oxides determined by XRF at the University of Massachusetts Amherst; reported in Damasceno (1996)
Analytical conditions and precision/accuracy of the XRF method are discussed in Rhodes (1988)
[a]Mg# = $Mg/(Mg + Fe^{2+})$
[b]AI = total alkalis−(SiO_2×0.37–14.43)

liners were used for all piston-cylinder experiments and possible Ba contamination of the sample was checked by random analyses by electron microprobe of Ba within the experimental glasses. These analyses indicated that contamination was rare and limited to those samples where fracturing of the graphite capsule was evident in thin section. Graphite furnaces were inserted into the sleeves, and the graphite capsules with lids, machined for a tight fit, and mullite spacers were placed inside the furnaces. An alumina disk separated the thermocouple from the graphite capsule. The use of graphite capsules constrained the f_{O2} to be at or below the GCO (graphite-C-O fluid) buffer. At our experimental conditions, f_{O2} probably varied between 0 and 2 log units below FMQ. Temperature was monitored with a $Pt–Pt_{90}Rh_{10}$ thermocouple and the temperature calibration for the assembly yielded a 14°C positive gradient from the thermocouple to the center of the capsule. Temperatures reported here are those at the hot spot. Pressure calibration of the cells using the reaction Mg-cordierite = sapphirine + quartz (Newton et al. 1974) at 0.7 GPa yielded a 0.07 GPa negative correction. Although this correction is probably somewhat pressure sensitive, it was assumed here that this pressure correction is appropriate for all pressures within the range 0.4–1.5 GPa.

Two sets of experiments were run at the higher pressures: nominally dry and hydrous experiments. The dry experiments were performed with graphite capsules containing the samples and, together, were dried at 800°C for 20 min in the presence of an Fe oxygen getter. The hydrous experiments used the structurally bound water in the natural sample instead of added water as the starting point. Micro-FTIR analysis of a super liquidus glass (Run 22) indicated a water content of 1.2–1.3 wt.%. Measured volatile contents in 34 Ma submarine basaltic glasses from ODP Leg 183 Site 1140 on the Northern Kerguelen Plateau give 0.23–0.26 wt.% H_2O for tholeiitic basalts ($K_2O = 0.16–0.18$ wt.%; $CO_2 = 42–55$ ppm) and up to 0.69 wt.% H_2O for the more alkali-rich tholeiitic-transitional basalts ($K_2O = 0.89$ wt.%; $CO_2 < 20–34$ ppm) (Wallace 2002). The K_2O content of the starting material in this study is 0.96 wt.% (Table 1), which would correspond to pre-eruptive H_2O contents of 0.9–1.0 wt.% based on the H_2O-K_2O relationship for Kerguelen basalt glasses from Wallace (2002), and is only slightly lower than the water contents of the hydrous experiments in this study.

Analytical methods

After each run, the graphite capsule was extracted from the experimental cell and cut in half along the vertical axis with a diamond-embedded sawblade. A polished thin section (~30 microns thick) was made from each run and the capsule, glass, and crystallized phases were examined in detail in both transmitted and reflected light. Major element compositions of minerals and quenched glasses in the experimental products were determined with a Cameca SX-50 electron microprobe at the Laboratoire de Minéralogie-Cristallographie de l'Université de Pierre et Marie Curie (Paris 6). Analytical conditions were an accelerating voltage of 30 kV and a 10 nA slightly defocused beam for the glasses (5 s counting time), and 15 kV and a 10 nA focused beam for the crystalline phases (10 s counting time). Data reduction and matrix corrections were made on-line using the PAP method. The good agreement between compositions of the glasses in the nine supra-liquidus runs (1, 2, 7, 8, 12, 15, 22, 23, 29) determined by electronprobe microanalysis and the whole rock composition determined by XRF (University of Massachusetts Amherst), including Na_2O, indicates that these analytical conditions are adequate for the nominally dry to slightly hydrous basaltic compositions considered in this study (Tables 1, 3). A few additional mineral analyses were determined with a Cameca SX-50 electron microprobe at the University of British Columbia (accelerating voltage of 15 kV, beam current of 20 nA, and spot size of 5 μm). Infrared spectroscopic measurements were conducted in transmittance mode using a Nicolet 20 SXB FTIR spectrometer attached to a Spectra Tech IR Plan microscope at the American Museum of Natural History, New York. The thickness of the experimental glass was measured using a Mitutoyo digimatic indicator and the total dissolved water concentration was determined from the intensity of the broad band at 3,570 cm^{-1}. Total water concentration was calculated using the method described in Dixon et al. (1995) and Mandeville et al. (2002).

Results

The experimental conditions, run durations, phase assemblages and phase proportions are summarized in Table 2. The average compositions of minerals and glasses from the experiments are reported in Table 3. To obtain the phase proportions from the phase compositions of Table 3, we used a mass balance technique (Bryan et al. 1969) where all of the analyzed elements were included. The residuals are generally low (Table 2) and confirm the fact that the capsules behaved as closed systems. The extent of possible Fe loss in the 0 GPa runs was evaluated by adding a fictive FeO "phase" in the crystalline assemblage for the least-squares regressions; no observable changes to the residuals were noted and therefore Fe loss was minor in these experiments.

Attainment of equilibrium

All phase equilibrium experiments presented here are crystallization experiments in which the starting material was heated well above the liquidus for at least 2 h before the temperature was dropped to the desired value at a cooling rate ranging from 0.4 to

Table 2 Experimental run conditions, phase assemblages and proportions

Run no.	Pressure (GPa)	Temp. (°C)	Time (hrs)	Water[a]	Run products[b]	Phase proportions[c] (wt.%)	Σr^2	Kd[d]		Mg# glass
								cpx/liq	plag/liq	
1	0.0	1,224	3	DRY	gl	100.0	–	–	–	0.43
7[e]	0.0	1,184	6	DRY	gl, pl	–	–	–	–	0.42
3	0.0	1,154	36	DRY	gl, pl	95.0:5.2	0.36	–	1.00	0.42
14	0.0	1,134	73	DRY	gl, pl	87.3:13.1	0.28	–	0.91	0.42
11	0.0	1,119	65	DRY	gl, pl, cpx, ol, tmt	77.7:19.0:2.9:0.4: tr	0.13	0.24	0.83	0.40
27	0.0	1,105	90	DRY	gl, pl, cpx, tmt	55.4:23.9:16.3:4.4	0.04	0.27	1.18	0.39
9	0.0	1,084	70	DRY	gl, pl, cpx, tmt	39.2:30.5:23.7:6.1	0.21	0.31	1.49	0.36
8	0.43	1,250	2	DRY	gl	100.0	–	–	–	0.44
15	0.43	1,200	2	DRY	gl	100.0	–	–	–	0.43
16	0.43	1,180	97	DRY	gl, pl, cpx	93.2:5.8:0.8	0.09	0.25	0.83	0.43
13	0.43	1,150	63	DRY	gl, pl, cpx	62.9:22.3:14.2	0.17	0.24	0.96	0.34
20	0.43	1,120	62	DRY	gl, pl, cpx, ol	46.0:32.0:19.8:2.2	0.26	0.20	0.82	0.27
2	0.93	1,280	2	DRY	gl	100.0	–	–	–	0.43
12	0.93	1,250	4	DRY	gl	100.0	–	–	–	0.43
10	0.93	1,210	49	DRY	gl, pl, cpx	74.9:10.8:14.1	0.06	0.23	0.62	0.35
4	0.93	1,180	61	DRY	gl, pl, cpx	46.2:27.0:27.4	0.50	0.22	0.70	0.27
19	0.93	1,160	92	DRY	gl, pl, cpx, ap	44.3:28.2:27.8: tr	0.24	0.21	0.70	0.26
23	1.43	1,300	2	DRY	gl	100.0	–	–	–	0.42
21[e]	1.43	1,270	2	DRY	gl, pl, cpx	–	–	–	–	–
24	1.43	1,250	96	DRY	gl, pl, cpx	70.2:7.7:22.2	0.27	0.27	0.59	0.32
26	1.43	1,220	65	DRY	gl, pl, cpx	50.9:19.4:29.3	0.29	0.24	0.55	0.27
30	1.43	1,190	69	DRY	gl, pl, cpx	35.4:27.9:36.4	0.21	0.26	0.45	0.23
22	0.43	1,180	2	HYDR	gl	100.0	–	–	–	0.42
37	0.43	1,050	50	HYDR	gl, cpx, plag, ilm	59.3:22.8:16.7:1.0	0.35	0.19	1.13	0.25
35	0.68	1,020	44	HYDR	gl, cpx, pl, ilm	47.2:31.9:18.3:2.4	0.05	0.18	1.11	0.22
29	0.93	1,220	2	HYDR	gl	100.0	–	–	–	0.43
31	0.93	1,120	63	HYDR	gl, cpx	80.6:19.1	0.09	0.23		0.33
38	0.93	1,000	43	HYDR	gl, cpx, pl, krs, ilm	39.7:32.7:13.6:12.1:1.8	0.09	0.11	1.06	0.16

[a]Water contents refers to experiments performed at either nominally dry (DRY) or hydrous (HYDR) conditions
[b]*gl* glass, *pl* plagioclase, *cpx* clinopyroxene, *ol* olivine, *tmt* titanomagnetite, *ilm* ilmenite, *krs* kaersutite, *ap* apatite
[c]Phase proportions were calculated by least square analysis considering all of the oxides
[d]Calculated as molar FeOsol*MgOliq/FeOliq*MgOsol for cpx/liq
[e]Incompletely melted runs used to help position liquidus; only glass composition analyzed

1.8°C/min. Run durations for the crystallization parts of the experiments varied between 36 h for near-liquidus runs to 97 h for lower temperature runs (Table 2) and the degree of crystallinity was kept low (melt fraction above 35–40 vol.%) to aid in the attainment of equilibrium between the melt and the crystalline phases. Several lines of evidence suggest that equilibrium was attained in our experiments. (1) Glass compositions are homogeneous throughout the capsules, even in the lower temperature, more crystallized experiments. (2) Backscattered electron images reveal that no quench crystals were formed as the runs were brought back to ambient pressure and temperature conditions. (3) Crystals are euhedral and show limited compositional variations with respect to their major element constituents. Plagioclase core-to-rim zoning is typically about 1 mol.% An and grain-to-grain variation within a single capsule is minor (typically about 1–2 mol.% An). Core-to-rim variations in the Mg# of clinopyroxene are typically 0.01–0.02, with local examples up to 0.05–0.08. (4) Clinopyroxene-melt Fe-Mg exchange distribution coefficients ($K_D^{Fe\text{-}Mg}$) are 0.25 ± 0.03 (1σ) for the dry experiments, which is within the range determined for other experimental studies (e.g., Hoover and Irvine 1977; Grove and Bryan 1983; Sisson and Grove 1993; Toplis and Carroll 1995; Putirka 1999), and 0.18 ± 0.05 (1σ) for the hydrous experiments (Table 2), which suggests that water in mildly alkalic basaltic melts affects Fe-Mg partitioning between clinopyroxene and melt. (5) Plagioclase-melt Ca-Na exchange distribution coefficients ($K_D^{Ca\text{-}Na}$) are similar to published values from other experimental studies at similar conditions (e.g., Grove and Baker 1984; Sisson and Grove 1993; Toplis and Carroll 1995). Values of $K_D^{Ca\text{-}Na}$ are relatively constant for each liquid-line-of-descent. For the dry experiments, $K_D^{Ca\text{-}Na}$ is 0.98 ± 0.15 at 0 GPa, which overlaps with the value (1.1 ± 0.2) determined by Toplis and Carroll (1995) for proposed parent magma compositions to the Skaergaard intrusion (very similar to the starting composition in this study). Values of $K_D^{Ca\text{-}Na}$ decrease with increasing pressure (0.87 ± 0.08 at 0.43 GPa, 0.67 ± 0.05 at 0.93 GPa, 0.53 ± 0.07 at 1.43 GPa [errors are 1σ]). For the hydrous experiments, the plagioclase $K_D^{Ca\text{-}Na}$ appears to be pressure insensitive and has a value of 1.10 ± 0.03 (1σ), which is

Table 3 Electron microprobe analyses of run products (in wt.% oxides)

Run #	Phase	Analyses #	Pressure GPa	Temp. °C	Water	SiO_2	2s	TiO_2	2s	Al_2O_3	2s	FeO	2s	MnO	2s	MgO	2s	CaO	2s	Na_2O	2s	K_2O	2s	P_2O_5	2s	Total	Mg#	Plag An%
1	Glass	5	0	1,220	DRY	50.02	0.65	2.76	0.07	14.89	0.16	11.82	0.35	0.20	0.01	4.99	0.15	10.28	0.31	2.85	0.06	0.93	0.07	0.65	0.11	99.39	0.43	–
7	Glass	3	0	1,184	DRY	50.00	0.46	2.70	0.01	14.91	0.14	12.41	0.37	0.19	0.02	5.05	0.14	10.31	0.07	2.78	0.33	0.92	0.05	0.75	0.06	100.03	0.42	–
3	Glass	5	0	1,154	DRY	50.25	0.65	2.80	0.30	14.59	0.57	12.96	0.40	0.20	0.07	5.20	0.33	10.17	0.27	2.69	0.06	0.94	0.07	0.74	0.08	100.54	0.42	–
	Plag	6	–	–	–	51.81	0.79	–	–	29.32	0.65	1.40	0.31	–	–	0.20	0.04	13.55	0.73	3.59	0.25	0.20	0.05	–	–	100.08	0.21	66.8
14	Glass	4	0	1,134	DRY	49.75	0.26	3.10	0.19	13.19	0.39	13.87	0.19	0.20	0.08	5.73	0.20	10.02	0.19	2.66	0.35	1.04	0.04	0.72	0.12	100.28	0.42	–
	Plag	6	–	–	–	52.00	0.76	–	–	28.82	0.83	1.43	0.34	–	–	0.24	0.09	13.12	0.64	3.81	0.30	0.23	0.06	–	–	99.66	0.23	64.7
11	Glass	3	0	1,119	DRY	49.51	0.22	3.39	0.13	12.29	0.37	14.62	0.19	0.24	0.07	5.56	0.25	9.73	0.31	2.55	0.39	1.07	0.11	0.74	0.18	99.70	0.40	–
	Plag	6	–	–	–	52.54	1.07	–	–	28.49	0.88	1.55	0.21	–	–	0.23	0.05	12.69	0.32	4.01	0.26	0.25	0.08	–	–	99.75	0.21	62.7
	Cpx	4	–	–	–	50.07	4.07	1.26	0.80	3.08	2.23	10.33	0.31	0.25	0.09	16.24	3.54	18.16	3.35	0.28	0.14	–	–	–	–	99.66	0.74	–
	Oliv	4	–	–	–	38.33	0.61	–	–	–	–	22.32	0.30	0.35	0.04	38.92	0.36	0.35	0.03	–	–	–	–	–	–	100.26	0.76	–
	Tmt	10	–	–	–	–	–	9.14	0.28	4.06	0.37	74.72	1.25	0.23	0.05	5.20	0.50	–	–	–	–	–	–	–	–	93.58	0.11	–
27	Glass	3	0	1,105	DRY	53.30	0.40	3.39	0.18	13.02	0.40	11.34	0.69	0.23	0.01	4.08	0.40	7.76	0.12	3.18	0.23	1.71	0.05	0.95	0.04	98.97	0.39	–
	Plag	3	–	–	–	52.66	0.63	–		27.40	0.49	1.55	0.26	–	–	0.31	0.10	12.25	0.59	4.26	0.40	0.25	0.02	–	–	98.67	0.26	60.5
	Cpx	10	–	–	–	47.10	2.12	2.15	0.75	5.20	1.67	10.79	0.66	0.24	0.09	14.16	1.34	18.89	1.25	0.36	0.04	–	–	–	–	98.89	0.70	–
	Tmt	12	–	–	–	–	–	12.31	0.55	3.67	0.37	71.24	1.33	0.42	0.07	5.31	0.63	–	–	–	–	–	–	–	–	93.04	0.12	–
9	Glass	4	0	1,080	DRY	57.29	1.06	3.03	0.07	12.90	0.55	9.39	0.58	0.20	0.10	3.01	0.19	6.25	0.50	3.29	0.32	2.35	0.07	1.09	0.10	98.79	0.36	–
	Plag	12	–	–	–	53.61	0.60	–	–	27.65	0.19	2.00	0.24	–	–	0.30	0.11	12.19	0.47	4.32	0.32	0.32	0.06	–	–	100.40	–	59.8
	Cpx	4	–	–	–	47.50	1.75	2.27	0.79	4.88	1.51	12.73	1.04	0.31	0.08	13.19	0.60	18.09	1.13	0.38	0.07	–	–	–	–	99.35	0.65	–
	Tmt	13	–	–	–	–	–	15.00	0.41	3.05	0.22	69.25	0.72	0.39	0.04	4.51	0.33	–	–	–	–	–	–	–	–	92.25	0.10	–
8	Glass	5	0.43	1,250	DRY	49.42	0.67	2.79	0.17	15.13	0.44	11.95	0.95	0.16	0.05	5.21	0.29	10.33	0.27	2.94	0.25	0.92	0.09	0.70	0.20	99.55	0.44	–
15	Glass	2	0.43	1,200	DRY	49.69	0.18	2.77	0.10	15.21	0.29	12.08	0.12	0.17	0.03	5.11	0.16	10.28	0.12	2.76	0.40	0.91	0.02	0.69	0.15	99.66	0.43	–
16	Glass	3	0.43	1,180	DRY	49.60	0.16	2.88	0.14	14.33	0.65	12.74	0.92	0.21	0.05	5.35	0.26	10.18	0.08	3.09	0.12	0.95	0.08	0.71	0.12	100.03	0.43	
	Plag	6	–	–	–	53.92	0.75	–	–	29.33	0.58	0.27	0.07	–	–	0.17	0.03	12.16	0.57	4.43	0.35	0.29	0.05	–	–	100.57	0.53	59.2
	Cpx	3	–	–	–	51.80	1.70	1.55	1.09	3.62	2.75	8.89	1.01	0.19	0.08	15.21	1.76	18.80	1.29	0.36	0.15	–	–	–	–	100.43	0.75	–
13	Glass	4	0.43	1,150	DRY	48.46	0.72	3.73	0.19	12.97	0.29	16.17	0.30	0.22	0.02	4.66	0.32	8.53	0.26	3.21	0.27	1.32	0.03	0.76	0.20	100.03	0.34	–
	Plag	6	–	–	–	54.31	1.18	–	–	28.71	1.03	0.39	0.16	–	–	0.18	0.04	11.76	0.39	4.63	0.18	0.36	0.07	–	–	100.34	0.45	57.2
	Cpx	6	–	–	–	50.88	1.37	1.86	0.54	3.59	1.12	12.13	1.82	0.24	0.08	14.84	1.06	16.61	2.74	0.32	0.05	–	–	–	–	100.48	0.69	–
20	Glass	3	0.43	1,120	DRY	46.34	0.41	4.84	0.33	11.98	0.18	18.46	0.41	0.27	0.09	3.86	0.21	8.15	0.16	2.99	0.27	1.51	0.13	0.94	0.05	99.33	0.27	–
	Plag	5	–	–	–	54.30	0.60	–	–	28.16	0.24	0.65	0.41	–	–	0.19	0.11	10.98	0.58	4.94	0.35	0.48	0.19	–	–	99.70	0.34	53.6
	Cpx	5	–	–	–	49.44	2.52	2.12	1.33	3.52	2.10	12.81	3.48	0.28	0.09	13.63	2.32	16.91	4.55	0.32	0.14	–	–	–	–	99.04	0.65	–
	Oliv	14	–	–	–	34.93	0.67	–	–	–	–	38.23	1.79	0.45	0.08	24.85	1.33	0.42	0.07	–	–	–	–	–	–	98.89	0.54	–
2	Glass	4	0.93	1,280	DRY	49.43	0.28	2.74	0.20	14.99	0.34	11.85	0.28	0.20	0.04	4.99	0.38	10.44	0.27	2.82	0.17	0.93	0.10	0.66	0.20	99.04	0.43	–
12	Glass	4	0.93	1,250	DRY	49.21	0.53	2.68	0.17	15.08	0.18	12.50	0.56	0.18	0.05	5.20	0.20	10.40	0.11	2.88	0.15	0.90	0.01	0.66	0.10	99.68	0.43	
10	Glass	9	0.93	1,210	DRY	49.20	0.51	3.11	0.10	14.77	0.35	14.18	0.36	0.20	0.04	4.37	0.11	9.07	0.29	2.95	0.07	1.07	0.09	0.77	0.07	99.70	0.35	–
	Plag	6	–	–	–	55.59	0.73	–	–	27.73	0.67	0.38	0.13	–	–	0.10	0.04	10.18	0.52	5.34	0.32	0.56	0.06	–	–	99.89	0.32	49.6
	Cpx	7	–	–	–	49.12	0.65	1.72	0.29	7.63	0.68	9.34	0.90	0.19	0.08	12.69	0.58	18.40	0.32	0.68	0.06	–	–	–	–	99.76	0.71	–
4	Glass	6	0.93	1,180	DRY	46.37	0.61	4.63	0.30	13.01	0.38	18.16	0.54	0.25	0.06	3.77	0.40	8.04	0.19	2.88	0.35	1.50	0.11	0.94	0.10	99.55	0.27	–
	Plag	5	–	–	–	56.26	0.35	–	–	28.01	0.31	0.73	0.25	–	–	0.13	0.05	10.18	0.26	5.20	0.27	0.80	0.18	–	–	101.29	0.24	49.6
	Cpx	11	–	–	–	47.48	1.38	2.10	0.89	7.51	2.28	12.98	2.58	0.25	0.09	12.48	1.36	15.77	2.77	0.61	0.11	–	–	–	–	99.19	0.63	–
19	Glass	3	0.93	1,160	DRY	46.15	0.47	4.92	0.17	12.76	0.29	18.02	0.41	0.21	0.07	3.55	0.15	7.88	0.05	2.91	0.11	1.47	0.16	0.90	0.08	98.76	0.26	–
	Plag	6	–	–	–	55.61	0.92	–	–	27.22	1.39	0.76	0.71	–	–	0.14	0.21	9.90	0.98	5.24	0.42	0.84	0.28	–	–	99.71	0.25	48.6
	Cpx	11	–	–	–	47.34	2.18	2.12	0.97	7.03	2.53	13.46	2.15	0.27	0.10	12.65	1.41	15.39	2.05	0.56	0.12	–	–	–	–	98.82	0.63	–
	+ Ap	–	–	–	–	–	–	–	–	–	–	–	–	–	–	–	–	–	–	–	–	–	–	–	–	–	–	–
23	Glass	4	1.43	1,300	DRY	49.69	0.55	2.66	0.14	15.03	0.25	12.53	0.22	0.21	0.09	5.14	0.15	10.28	0.21	2.81	0.21	0.88	0.08	0.70	0.14	99.93	0.42	–
24	Glass	7	1.43	1,250	DRY	48.35	1.12	3.56	0.40	14.93	0.53	13.84	0.60	0.18	0.09	3.62	1.23	8.12	1.23	3.36	0.49	1.24	0.18	0.73	0.12	97.92	0.32	–
	Plag	6	–	–	–	57.92	0.89	–	–	26.93	0.36	0.33	0.10	–	–	0.06	0.02	8.74	0.40	6.12	0.35	0.77	0.15	–	–	100.87	0.26	42.2
	Cpx	4	–	–	–	48.30	0.67	1.59	0.09	9.35	0.87	11.27	0.49	0.22	0.09	11.10	0.49	17.41	0.29	1.22	0.13	–	–	–	–	100.46	0.64	–

Table 3 (Contd.)

Run #	Phase	Analyses #	Pressure GPa	Temp. °C	Water	SiO_2	2s	TiO_2	2s	Al_2O_3	2s	FeO	2s	MnO	2s	MgO	2s	CaO	2s	Na_2O	2s	K_2O	2s	P_2O_5	2s	Total	Mg#	Plag An%
26	Glass	5	1.43	1,220	DRY	48.24	0.97	4.45	0.15	14.04	0.35	16.48	0.29	0.23	0.08	3.34	0.14	7.73	0.24	2.99	0.42	1.47	0.17	0.85	0.13	99.81	0.27	–
	Plag	6	–	–	–	58.02	0.72	–	–	26.31	0.23	0.49	0.24	–	–	0.08	0.01	8.63	0.13	6.09	0.15	0.97	0.22	–	–	100.60	0.22	41.5
	Cpx	5	–	–	–	48.32	2.30	1.74	0.90	8.52	3.31	13.42	3.08	0.24	0.08	11.31	1.44	15.76	1.52	1.04	0.18	–	–	–	–	100.35	0.60	–
30	Glass	4	1.43	1,190	DRY	45.60	0.98	5.89	0.49	13.26	0.35	18.35	0.26	0.24	0.03	3.10	0.22	7.75	0.29	2.50	0.17	1.52	0.04	1.21	0.27	99.42	0.23	–
	Plag	6	–	–	–	58.47	0.87	–	–	26.05	0.60	0.48	0.09	–	–	0.07	0.05	8.25	0.53	5.94	0.18	1.49	0.20	–	–	100.74	0.19	39.7
	Cpx	6	–	–	–	47.90	0.57	1.93	0.16	8.07	1.20	16.06	1.87	0.27	0.06	10.47	0.33	14.88	1.21	0.96	0.14	–	–	–	–	100.55	0.54	–
22	Glass	3	0.43	1,180	HYDR	49.51	0.61	2.79	0.13	14.97	0.04	12.01	0.50	0.19	0.05	4.89	0.26	10.13	0.13	2.95	0.45	0.95	0.03	0.62	0.11	99.01	0.42	–
37	Glass	5	0.43	1,050	HYDR	47.97	1.64	2.82	0.34	14.57	0.21	14.57	0.75	0.18	0.05	2.73	0.40	7.22	0.23	3.34	0.26	1.52	0.14	0.83	0.19	95.75	0.25	–
	Cpx	6	–	–	–	49.13	1.95	1.95	0.68	5.16	2.47	11.94	2.23	0.22	0.07	11.99	1.98	18.19	2.17	0.44	0.25	–	–	–	–	99.02	0.64	–
	Plag	8	–	–	–	53.42	0.72	–	–	28.79	0.85	0.36	0.19	–	–	0.08	0.03	11.40	0.83	4.69	0.28	0.31	0.11	–	–	99.05	0.29	56.3
	Ilm	10	–	–	–	–	–	51.82	0.38	0.34	0.07	40.58	0.52	0.45	0.09	3.81	0.08	–	–	–	–	–	–	–	–	97.07	0.14	–
35	Glass	5	0.68	1,020	HYDR	50.00	0.56	1.65	0.06	15.62	0.39	13.68	0.65	0.18	0.07	2.17	0.23	6.05	0.17	3.58	0.43	1.84	0.07	0.87	0.12	95.64	0.22	–
	Cpx	9	–	–	–	47.10	3.53	2.27	1.59	7.17	4.30	13.18	5.53	0.25	0.12	11.58	1.90	16.71	3.07	0.50	0.20	–	–	–	–	98.77	0.61	–
	Plag	5	–	–	–	55.27	1.62	–	–	27.80	1.08	0.55	0.23	–	–	0.06	0.04	10.17	1.32	5.41	0.48	0.41	0.09	–	–	99.67	0.16	49.7
	Ilm	9	–	–	–	–	–	50.11	0.38	0.45	0.15	42.20	0.35	0.31	0.03	2.80	0.12	–	–	–	–	–	–	–	–	95.90	0.11	–
29	Glass	4	0.93	1,220	HYDR	48.85	0.68	2.77	0.06	14.76	0.20	12.02	0.37	0.18	0.07	5.00	0.27	10.26	0.20	2.75	0.15	0.91	0.10	0.65	0.13	98.16	0.43	–
31	Glass	4	0.93	1,120	HYDR	48.47	0.39	2.86	0.18	15.69	0.42	12.21	0.30	0.20	0.08	3.30	0.12	8.08	0.16	3.24	0.19	1.13	0.03	0.68	0.13	95.86	0.33	–
	Cpx	11	–	–	–	47.37	1.88	2.03	0.94	8.38	2.17	10.18	0.85	0.21	0.06	11.73	1.12	18.54	0.83	0.66	0.12	–	–	–	–	99.11	0.67	–
38	Glass	5	0.93	1,000	HYDR	53.17	0.41	1.10	0.11	15.93	0.29	12.26	0.68	0.15	0.10	1.34	0.15	5.39	0.08	3.77	0.40	2.19	0.11	1.04	0.18	96.35	0.16	–
	Cpx	9	–	–	–	46.68	1.13	2.47	0.60	9.10	1.21	11.32	3.56	0.21	0.08	10.92	1.46	18.08	1.72	0.72	0.09	–	–	–	–	99.50	0.63	–
	Plag	6	–	–	–	56.86	0.74	–	–	27.39	1.18	0.54	0.11	–	–	0.03	0.03	9.11	0.92	6.01	0.51	0.49	0.14	–	–	100.44	0.10	44.3
	Kaers	13	–	–	–	38.49	0.52	5.26	0.91	13.83	0.39	20.75	0.78	0.22	0.07	7.17	0.39	8.78	0.42	2.51	0.13	0.70	0.13	–	–	97.87	0.38	–
	Ilm	10	–	–	–	–	–	49.32	0.57	0.51	0.19	44.60	0.80	0.36	0.09	1.78	0.08	–	–	–	–	–	–	–	–	96.58	0.07	–

consistent with relatively low water contents (< 2 wt.%; Sisson and Grove 1993).

Phase relations

The near-liquidus phase assemblages as a function of pressure and temperature for both the dry and hydrous experiments are reported in Fig. 3. The sequence of crystallization at 0 GPa is plagioclase, clinopyroxene, olivine, titanomagnetite, olivine-out (Fig. 3a). At higher pressures, olivine is not stable at any of the experimental conditions. The crystallization sequence for dry conditions at higher pressures is generally similar to the dry low-pressure sequence, differing in that plagioclase and clinopyroxene co-crystallize throughout the range of examined pressure and temperature conditions. The proportion of plagioclase relative to clinopyroxene, however, decreases with increasing pressure (Table 2). The crystallization sequence of the hydrous experiments is quite different (Fig. 3b). Clinopyroxene is the dominant phase even at lower pressures, because the liquid is depolymerized by the presence of water, thus inhibiting the crystallization of plagioclase. At lower temperatures in the hydrous runs, ilmenite crystallizes, and finally a reddish, Ti-rich amphibole (kaersutite-ferrokaersutite), in the lowest temperature run (1,000°C) at 0.93 GPa.

Glass chemistry

Major element analyses of all glasses produced in the experiments are reported in Table 3 and trends are indicated in Fig. 4 with respect to MgO. The CaO content of the glasses decreases continuously for decreasing temperature at all experimental pressures and water contents, as the liquidus assemblage consists of plagioclase and/or clinopyroxene, both CaO-rich phases. At 0 GPa, progressive crystallization of the melt is characterized by an increase in the SiO_2, Na_2O, K_2O and P_2O_5 contents of the residual glasses. Initially, the crystallization of plagioclase as the only liquidus phase increases the FeO and MgO contents of the liquid and decreases Al_2O_3, with SiO_2 remaining relatively constant. After titanomagnetite saturation, around 20–25% crystallization, the liquid becomes enriched in SiO_2 (up to 57 wt.%), the Al_2O_3 content becomes constant and FeO and MgO decrease. The TiO_2 content stays relatively constant throughout the 0 GPa liquid-line-of-descent.

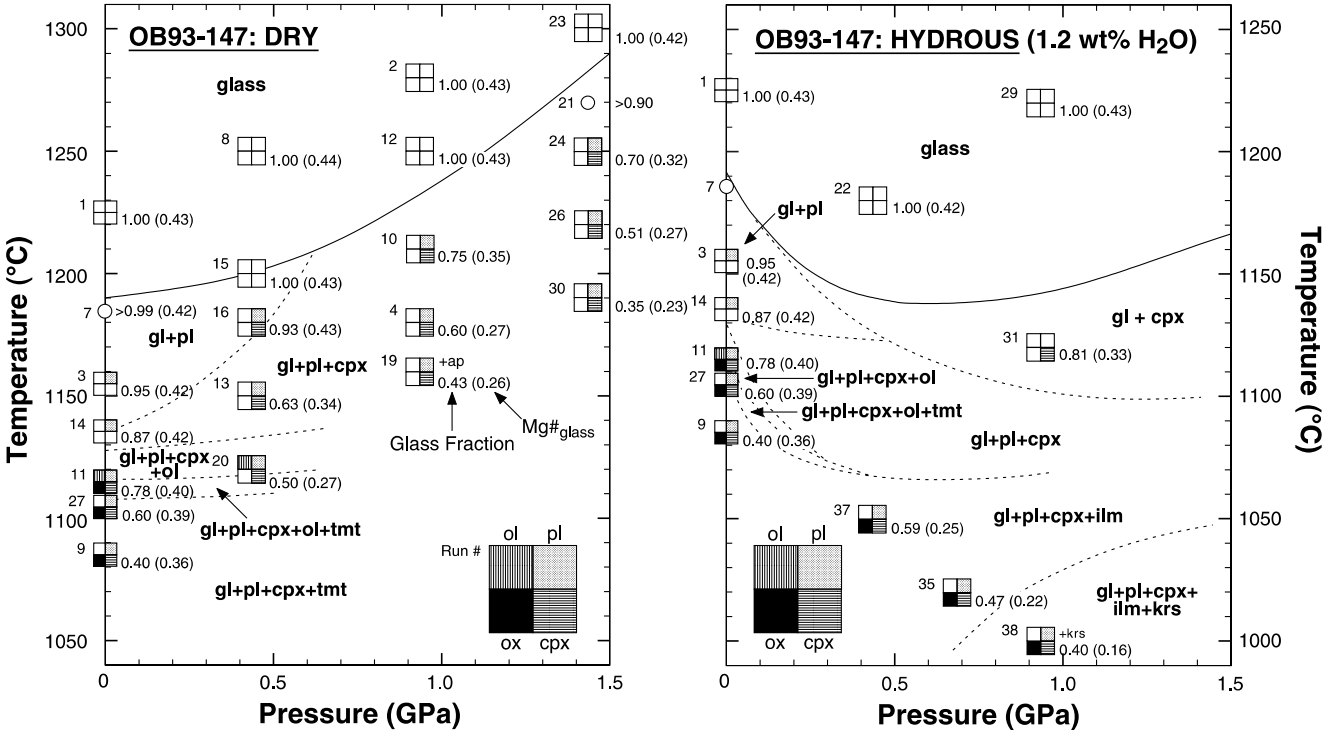

Fig. 3 Pressure-temperature phase diagrams showing the stability fields for the different phases present in the nominally dry experiments (*left*) and hydrous experiments (*right*). The 0 GPa results are indicated on the hydrous diagram for reference. Note the difference in temperature ranges for the two diagrams. The *boxes* are shaded to indicate the assemblage present in each run and the run numbers are indicated in adjacent to the upper left corner of each box. The fraction of glass in each run and the Mg# of the glass are shown adjacent to the lower right corner of each box. Runs #7 and #21 (*open circles*) are incompletely melted experiments containing 1–10% crystals and were used to position the liquidus. Abbreviations are as follows: *gl* glass, *pl* plagioclase, *cpx* clinopyroxene, *ol* olivine, *ilm* ilmenite, *tmt* titanomagnetite, *krs* kaersutite, *ap* apatite

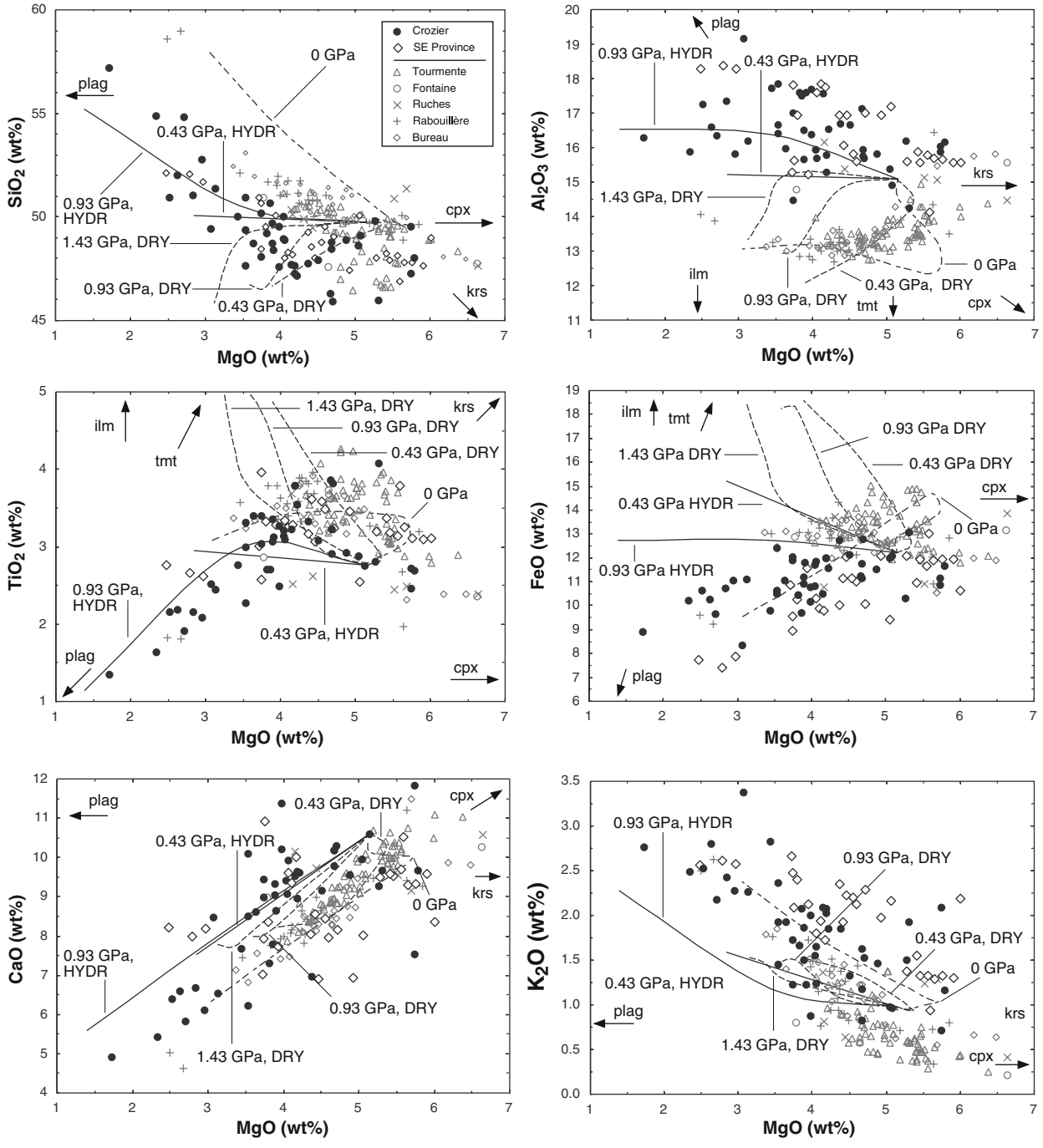

Fig. 4 Diagrams of MgO versus major element oxides (SiO_2, Al_2O_3, TiO_2, FeO, CaO, K_2O) showing the compositional variation of the glasses in the experiments at different pressures and water contents and the range of compositions of lavas from the Kerguelen Archipelago. The hydrous trends are shown as *black solid lines* and the nominally anhydrous and 0 GPa trends are shown as *dashed lines*. *Arrows* point towards the compositions of the major crystalline phases. The 24–25 Ma mildly alkalic series samples are indicated with slightly larger *black symbols* (*filled circles* and *open diamonds*). The 26–29 Ma tholeiitic-transitional series samples are indicated with the smaller *grey symbols*; the olivine-phyric high-MgO basalts (>7 wt.%) from the Bureau ($n=5$) and Rabouillère ($n=2$) sections (Yang et al. 1998) and from the Ruches ($n=13$) and Fontaine ($n=21$) sections (Doucet et al. 2002) have been omitted to allow for inspection of the crystallization trends emanating from the 5 wt.% MgO content of the starting composition (OB93–147). Data sources for the lava compositions are as indicated in the caption to Fig. 1b. The compositional variation of the Kerguelen Archipelago lavas on these diagrams is primarily a function of mineral fractionation as described in the source articles for the data from each basaltic section. Approximately 50% of the analyzed lavas are aphyric, and the remaining samples range from sparsely-phyric (<5 vol.% phenocrysts) to strongly porphyritic (up to 20 vol.% phenocrysts). The phenocryst assemblage is similar in both series, and is dominated by plagioclase for compositions <6 wt.% MgO ± clinopyroxene and olivine, with microphenocrysts of titanomagnetite and ilmenite present in samples with <4 wt.% MgO; samples with >17 wt.% Al_2O_3 have accumulated plagioclase. Note the clear distinction between the 24–25 Ma mildly alkalic series and 26–29 Ma transitional-tholeiitic series with respect to Al_2O_3 versus MgO and the corresponding difference between the dry and hydrous crystallization paths

The dry high-pressure compositional trends in the glass compositions are generally similar to those at 0 GPa in that early crystallization is dominated by plagioclase. The difference is that Fe-Ti oxides do not saturate in any of the high-pressure experiments and clinopyroxene is present in proportions that increase with increasing pressure. This results in a decrease of SiO_2, Al_2O_3 and MgO and an increase in FeO, TiO_2 and MnO in the residual glasses (Fig. 4). At 1.43 GPa, the Na_2O content of the glass increases (up to 3.3 wt.%) as clinopyroxene dominates the crystallizing assemblage, but at ~50% crystallization the mode of plagioclase increases by a factor of ~2.5 causing a drop in the Na_2O content of the glasses.

The liquid-line-of-descent of the hydrous experiments is very different from the dry experiments as near-liquidus plagioclase is not stable at pressures above ~0.5 GPa (Fig. 4). This results in a crystallization sequence and compositional trends that are dominated by clinopyroxene. As a result, the SiO_2, Na_2O and K_2O contents of the glasses increase, whereas the TiO_2, MnO, MgO contents decrease as crystallization proceeds. The Al_2O_3 content of the residual glasses remains effectively constant with decreasing temperature at 0.43 GPa and increases slightly with crystallization for the higher pressure 0.93 GPa experiments before leveling out at about 16.5 wt.% down to very low MgO contents (Fig. 4).

Mineral chemistry

Major element analyses of all the minerals present in the experiments are reported in Table 3 and plagioclase and clinopyroxene compositions are shown in Fig. 5. Average near-liquidus plagioclase compositions decrease systematically from An_{67} at 0 GPa to An_{42} at 1.43 GPa for the dry experiments. For the hydrous experiments, average near-liquidus plagioclase compositions decrease from An_{56} at 0.43 GPa to An_{44} at 0.93 GPa (Figs. 3, 5). There is a strong inverse correlation for plagioclase-liquid Ca-Na distribution with values of ~1 at 0 GPa to values of ~0.55 at 1.43 GPa for the dry experiments; for the hydrous experiments, values are approximately constant at 1.1 (Table 2).

There are strong pressure effects on the composition of clinopyroxene in the experiments. With respect to the quadrilateral components, there are general trends of decreasing Wo and increasing Fs with increasing pressure in both types of experiments (Fig. 5). Average Al_2O_3 contents increase with increasing pressure from 3.1–9.4 wt.% in the dry experiments and from 5.2–9.1 wt.% in the hydrous experiments. The Al^{VI} and Jd components in clinopyroxene increase systematically with increasing pressure from 0–0.22 and from 0–0.09, respectively.

Titanomagnetite is the stable Fe-Ti oxide in the dry experiments, but only at 0 GPa, and ilmenite is the stable Fe-Ti oxide in the higher pressure hydrous experiments (Fig. 3), reflecting the more oxidizing nature of the 0 GPa experiments ($Au_{80}Pd_{20}$ tube in evacuated silica glass tube) compared to the higher pressure experiments (graphite capsules and furnace in $BaCO_3$ sleeves). The titanomagnetite compositions change systematically with decreasing temperature from $Mt_{72.8}Usp_{27.2}$ at 1,119°C to $Mt_{54.9}Usp_{45.1}$ at

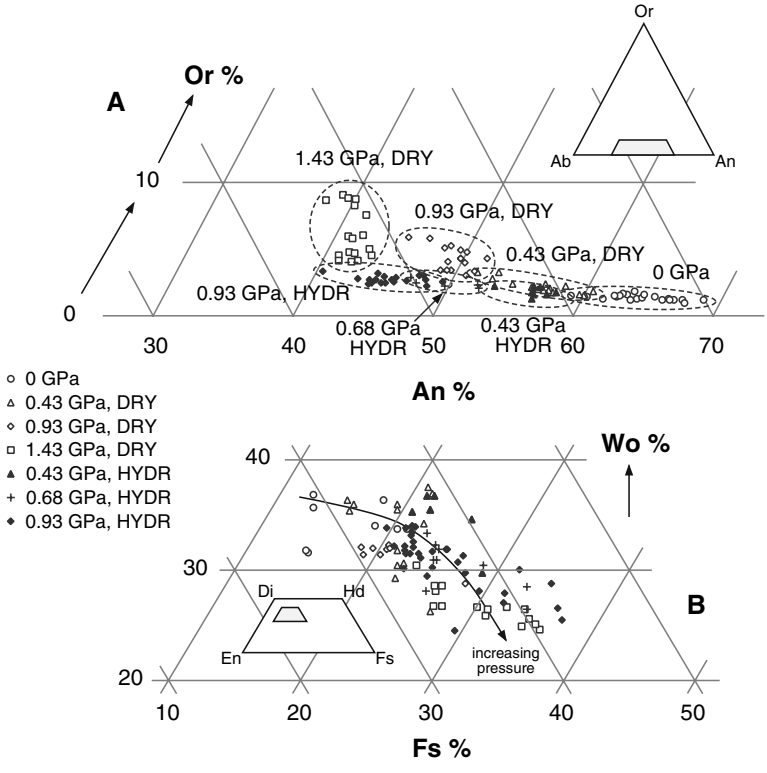

Fig. 5 **a** Expanded view of part of the An-Ab-Or feldspar ternary showing the compositions of plagioclase produced in the experiments. Individual point analyses are shown and grouped according to different pressures and water contents. Note the strong pressure control on plagioclase composition (decreasing An with increasing pressure). **b** Expanded view of part of the pyroxene quadrilateral showing the compositions of the clinopyroxenes produced in the experiments. Individual point analyses are shown. Increasing pressure results in clinopyroxene with higher Al_2O_3 contents, lower amounts of Wo component, and lower Mg#

1,080°C and the ilmenite compositions become slightly more hematite-rich with increasing pressure from $Ilm_{98.5}Hem_{1.5}$ at 0.43 GPa to $Ilm_{97.0}Hem_{3.0}$ at 0.68 GPa to $Ilm_{95.6}Hem_{4.4}$ at 0.93 GPa.

Discussion

The results of this experimental study on a transitional to mildly alkalic basalt from the Kerguelen Archipelago reveal that a relatively wide range of major element compositions can be produced through equilibrium crystallization of a single starting composition by varying pressure and water contents. This compositional diversity is reflected by systematic changes in the crystallization sequences with different pressures and water contents as described above, and in the compositions of the crystallizing phases themselves. Below, we compare the compositional trends produced in the experiments with the natural variation observed in the 24–29 Ma basalts from the Kerguelen Archipelago. We evaluate (1) the fractionation trends and crystallization conditions for these basalts, focusing on the differences between the tholeiitic-transitional basalts and the mildly alkalic basalts, (2) the role of fractionation alone in producing significant changes in the alkalinity of basalts from the archipelago, and (3) experimental constraints on crustal and lithospheric structure under the Kerguelen Archipelago with implications for the tectonic setting of the archipelago, melting conditions, and the evolution of the Kerguelen mantle plume-related volcanism.

Geochemical variations: experimental versus natural trends

Experimental crystallization trends for the different conditions determined in this study (0 GPa dry; 0.43 GPa dry; 0.93 GPa dry, 1.43 GPa dry; 0.43 GPa hydrous, 0.93 GPa hydrous) are shown compared to the compositional range of the 24–29 Ma basalts from the Kerguelen Archipelago in Fig. 4. Detailed geochemical studies of basaltic sections across the Kerguelen Archipelago, combined with $^{40}Ar/^{39}Ar$ dating, demonstrate that tholeiitic-transitional basalts were erupted in the central to northwestern parts of the archipelago from 26–29 Ma (Yang et al. 1998; Nicolaysen et al. 2000; Doucet et al. 2002; Frey et al. 2002) and that mildly alkalic basalts were erupted in the eastern and southeastern parts of the archipelago from 24–25 Ma (Weis et al. 1993; Frey et al. 2000a; Nicolaysen et al. 2000; Damasceno et al. 2002), including the Mont Crozier section on the Courbet Peninsula (Fig. 1b). The younger mildly alkalic lavas (mainly basalts and trachybasalts, but extending to trachytes) are characterized by increasing Al_2O_3, Na_2O, and K_2O contents, and decreasing TiO_2, FeO, and CaO contents, with decreasing MgO (a proxy for differentiation index or temperature of crystallization) (Fig. 4). The clearest distinction between the mildly alkalic and tholeiitic-transitional series on the archipelago resides in their Al_2O_3 contents relative to MgO, with the tholeiitic-transitional series extending to low Al_2O_3 contents (~13 wt.%) and the mildly alkalic series extending to higher Al_2O_3 contents (16–17 wt.%; Al_2O_3 contents higher than this reflect plagioclase accumulation in these rocks).

The experimental conditions that most closely reproduce the natural trends in the mildly alkalic series are those carried out at relatively high pressure (0.93 GPa) under slightly hydrous conditions (~1.2 wt.% H_2O) (Fig. 4). In particular, the trend of the 0.93 GPa hydrous experiments produces the characteristic Al- and Si-enrichment and Ti-depletion of this series of lavas. This indicates that fractionation in the mildly alkalic series was controlled primarily by segregation of high-Al clinopyroxene at depth, with a relatively minor role for plagioclase, a conclusion also reached by Damasceno et al. (2002) in their study of phenocryst compositions from the 24 Ma Mont Crozier lavas. The 0.93 GPa hydrous experiments, however, do not result in decreasing FeO contents with decreasing MgO, and although they produce increasing contents of the alkalis (Na_2O and K_2O) with crystallization, the experimental glasses are systematically lower in alkalis than the natural lavas. Fe-Ti oxide saturation in the Crozier series lavas occurs at ~4 wt.% MgO with the appearance of phenocrysts of both ilmenite and titanomagnetite (Damasceno et al. 2002), but the 0.93 GPa experiments produced only ilmenite (~2 wt.%) in the lowest temperature experiment (1,000°C). This resulted in a ratio of Fe:Ti for the crystallizing assemblage in the experiments that was much lower than that in the mildly alkalic basaltic magmas, where both Ti-rich (ilmenite) and Fe-rich (titanomagnetite) phenocrysts were crystallizing, and indicates that the f_{O2} conditions of the hydrous experiments (Δlog FMQ = 0–2) were more reduced than the prevailing f_{O2} in the natural magmas. The relatively reduced nature of the high-pressure experiments provide an upper limit of alkalinity increase per unit drop in temperature as higher f_{O2} will lead to more titanomagnetite crystallization, which will drive the residual liquid to higher SiO_2 contents (see following section). The systematically lower alkali contents in the 0.93 GPa hydrous experiments compared to the lavas are significant and are related to the maximum extent of alkali enrichment that can be produced through fractionation (see following section).

None of the crystallization sequences of the dry experiments at the different examined pressures (0, 0.43, 0.93, 1.43 GPa) is relevant to the compositional variation shown by the mildly alkalic series on the Kerguelen Archipelago (Fig. 4). However, at 0 GPa, the dry experiments produce trends that closely approximate some of the major element variations of the older tholeiitic-transitional basalts, particularly the decreasing Al_2O_3 and increasing SiO_2 contents with decreasing MgO. This observation is consistent with an important

role for plagioclase (±clinopyroxene-olivine) fractionation at relatively low pressure for the tholeiitic-transitional series on the archipelago. The higher pressure experiments under dry conditions are also notable for producing extreme Fe- and Ti-enrichment, up to 18 wt.% FeO and 5 wt.% TiO_2, and Si-depletion (down to 46 wt.% SiO_2) (Fig. 4). These experiments may have relevance to magma bodies where extreme Fe-enrichment during the latest stages of crystallization has been proposed (e.g., Skaergaard intrusion; Wager (1960), McBirney and Naslund (1990); Jang et al. (2001)). The f_{O2} conditions of these experiments were sufficiently reducing (log FMQ = 0 to −2) that the crystallization of ilmenite and titanomagnetite was suppressed, thus allowing for extensive Fe-enrichment of the residual glasses with no increase in SiO_2 content. This may also be the case at pressures less than 0.43 GPa, but the f_{O2} conditions of the 0 GPa experiments were sufficiently oxidizing (Δlog FMQ = +1 to +2) to stabilize magnetite early in the crystallization sequence.

Significance and extent of alkalinity variations

The starting basalt (OB93–147) for the experiments carried out in this study was chosen specifically because its total alkali content is such that it plots on the tholeiitic-alkalic dividing line of MacDonald and Katsura (1964) and the experiments were designed to test the extent of alkalinity variations possible by crystallization at different pressures and water contents. Can the range of alkalinity observed in the 24–29 Ma basalts from the Kerguelen Archipelago be explained by fractionation of a clinopyroxene-dominant assemblage as suggested for individual volcanoes on Galápagos (Naumann and Geist 1999) and Réunion (Albarède et al. 1997)?

The experimental crystallization trends are shown in Fig. 6 on a plot of total alkalis versus SiO_2, including the fields for the experimentally-produced clinopyroxene and plagioclase crystals. These trends are compared with the compositions of the 24–29 Ma basalts on the Kerguelen Archipelago, which are the same samples plotted in Fig. 4 (see caption to Fig. 4 for a brief description of the petrology and phenocryst assemblage of these samples). Although the 0.93 GPa hydrous experiments reproduce the main geochemical variations observed in the Mont Crozier section (Fig. 4), they are not associated with significant changes in alkalinity. This is due mainly to the effect of pressure and water content on the composition of the clinopyroxene that crystallizes in the experiments

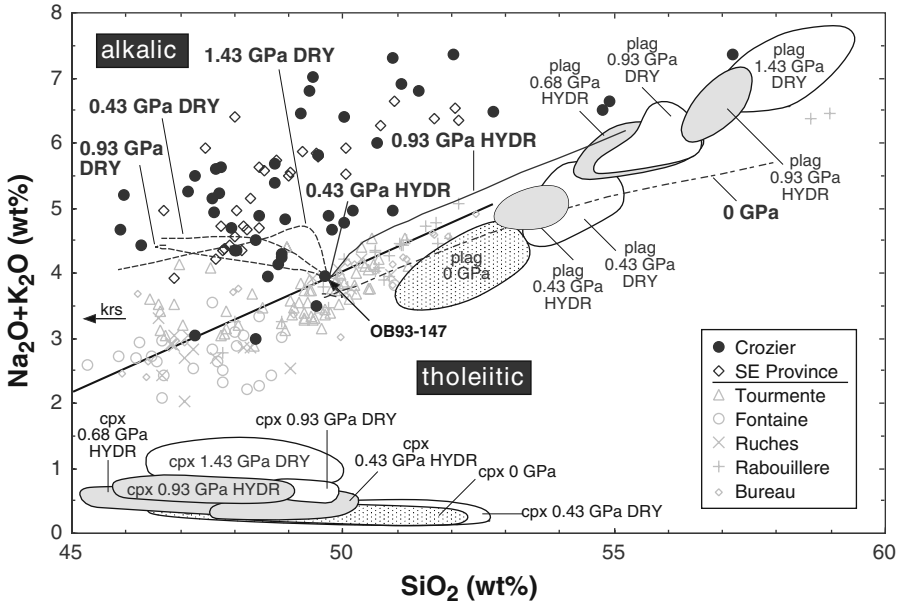

Fig. 6 Diagram of total alkalis ($Na_2O + K_2O$) versus SiO_2 showing the compositional variation of the glasses in the experiments at different pressures and water contents and the range of compositions of lavas from the Kerguelen Archipelago. The tholeiitic-alkalic boundary is from MacDonald and Katsura (1964). The hydrous trends are shown as *black solid lines* and the nominally anhydrous and 0 GPa trends are shown as *dashed lines*. The 24–25 Ma mildly alkalic series samples are indicated with slightly larger *black symbols* (*solid circles* and *open diamonds*) and the 26–29 Ma tholeiitic-transitional series samples are indicated with the smaller *grey symbols*. Data sources for the lava compositions are as indicated in the caption to Fig. 1b and discussion of the fractionation effects on the natural samples is in the caption to Fig. 4. Also shown are fields for clinopyroxene and plagioclase produced in the experiments grouped according to different pressures and water contents. The large range of alkalinity shown by the 24–25 Ma mildly alkalic basalts from Crozier and the Southeast Province is not reproduced by the experimental trends, especially the 0.93 GPa hydrous trend, which successfully reproduced the Al-enrichment with decreasing MgO in Fig. 4 that is typical of the mildly alkalic lavas. This is due primarily to the relatively low-Si content of the Al-rich clinopyroxene produced at this pressure, coupled with the onset of Fe-Ti oxide crystallization (ilmenite), that drives the residual melt composition to higher SiO_2 contents with only minor changes in alkalinity

(Fig. 6). Crystallization of relatively Si-rich, Al-poor clinopyroxene only under dry conditions and low pressures (0 and 0.43 GPa) would drive a starting composition like OB93-147 into the alkalic field. However, plagioclase is the dominant crystallizing phase under dry conditions, except at 1.43 GPa, and the residual glasses either show a small enrichment in total alkalis coupled with decreasing SiO_2 (0.43 GPa dry, 0.93 GPa dry) or a slight decrease in alkalis coupled with increasing SiO_2 (0 GPa), which is a function of early magnetite saturation in the 0 GPa experiments. At high pressures (0.68 and 0.93 GPa) and slightly hydrous conditions, relatively Si-poor, Al-rich clinopyroxene crystallizes. Because clinopyroxene is the main crystallizing phase in these experiments, formation of Si-poor, Al-rich clinopyroxene results in a subtraction vector at a high angle to the alkalic-tholeiitic boundary, producing Si-enrichment with minor increases in alkalinity. The 0.43 GPa hydrous experiments appear slightly more promising with respect to alkalinity changes, but fail to produce the Al-enrichment that is typical of the mildly alkalic series, and only cover a small range of the total alkalinity shown by the Mont Crozier basalts (Fig. 6).

The range of alkalinity defined by the transitional to mildly alkalic basalts from the Kerguelen Archipelago is clearly not reproduced by the experiments undertaken in this study, which cover a wide range of temperature, pressure and water contents. Based on the change from tholeiitic-transitional basaltic volcanism (26–29 Ma) to mildly alkalic basaltic volcanism (24–25 Ma) on the archipelago, coupled with higher Ce/Y, La/Yb and lower Zr/Nb in the mildly alkalic lavas, Weis et al. (1998a) and Frey et al. (2000a) proposed that the mildly alkalic series required a decrease in the extent of partial melting of the mantle beneath the archipelago and an increase in the proportion of residual garnet in the residue during melting. Our experiments support their proposal that significant changes in alkalinity primarily reflect changes in melting conditions and not fractionation of clinopyroxene, although clinopyroxene became the dominant crystallizing phase during evolution of the mildly alkalic series and controls much of the major element chemistry of the lavas (Damasceno et al. 2002; this study). Decreasing extents of partial melting of spinel lherzolite result in increased alkali contents in the melt with relatively high SiO_2 contents at low to moderate pressures (<1.5 GPa) (e.g., Baker and Stolper 1994; Kushiro 1996; Hirschmann et al. 1998a, 1998b). Longhi (2002) demonstrates that high alkali, low-SiO_2 melts, typical of many of the least-fractionated Crozier lava compositions (Fig. 6), are only possible in the garnet-lherzolite stability field, which is consistent with the requirement for garnet in the residue for the mildly alkalic basalts on the Kerguelen Archipelago (Weis et al. 1998a; Frey et al. 2000a).

Implications for crustal and lithospheric structure beneath the Kerguelen Archipelago

The results of this experimental study can also be used to place important constraints on both the crustal and lithospheric structure beneath the Kerguelen Archipelago. Seismic refraction studies indicate that the crust beneath the Northern Kerguelen Plateau is entirely oceanic in origin (i.e., there are no low-velocity zones that could be interpreted as representing continental material) (Recq et al. 1994; Charvis et al. 1995). The crust is divided into three major layers (Fig. 7a): (1) the 8–9 km thick upper crust with velocities similar to those of oceanic layer 2, (2) the 6–7 km thick lower crust with velocities comparable to oceanic layer 3, and (3) a high-velocity-gradient crust-to-mantle transition zone that has been interpreted as a 2–3 km thick zone of underplated material (Recq et al. 1994; Grégoire et al. 1998). Clinopyroxene-liquid thermobarometry and clinopyroxene structural barometry on phenocrysts and whole rocks from the Mont Crozier basaltic section indicate a role for high-pressure fractionation of high-Al clinopyroxene beneath the archipelago at 24 Ma (Damasceno et al. 2002), a conclusion that is reinforced by the results of this study. High-Al clinopyroxene may thus represent an important component of the crust-to-mantle transition zone at 14–16 km depth (Fig. 7a).

The change to mildly alkalic basaltic volcanism that is dominated by clinopyroxene fractionation at ~25 Ma on the Kerguelen Archipelago appears to be related to the increasing thickness of the crust beneath the archipelago and of the lithosphere beneath the Northern Kerguelen Plateau as the distance between the Kerguelen hotspot and the Southeast Indian Ridge increased (shown schematically in Fig. 7b). At ~43 Ma, Broken Ridge was separated from the Central Kerguelen Plateau by propagation of the Southeast Indian Ridge (Tikku and Cande 2000), the hotspot became ridge-centered, and the Northern Kerguelen Plateau began to form. At 34 Ma, tholeiitic pillow basalts sampled at ODP Leg 183 Site 1140 erupted, forming the lower parts of the Northern Kerguelen Plateau. This occurred when the ridge axis was ~50 km away (i.e., the hotspot was still effectively ridge-centered), a situation that would have allowed for extensive plume-ridge interaction and relatively thin crustal and lithospheric thicknesses (e.g., Ito et al., 2003). The source of these tholeiitic basalts is dominated by a Southeast Indian Ridge depleted mantle component (63–99%) (Weis and Frey 2002). Subsidence estimates for ODP Leg 183 Site 1140 based on vapor saturation pressures calculated using the H_2O and CO_2 contents of basaltic glass, and estimates from other ODP drilling sites on the Kerguelen Plateau, indicate that the various parts of the Kerguelen Plateau subsided at a rate comparable with that of normal Indian Ocean lithosphere (Wallace 2002). From 29 to 24 Ma, the distance between the archipelago and the ridge increased from ~200 km to

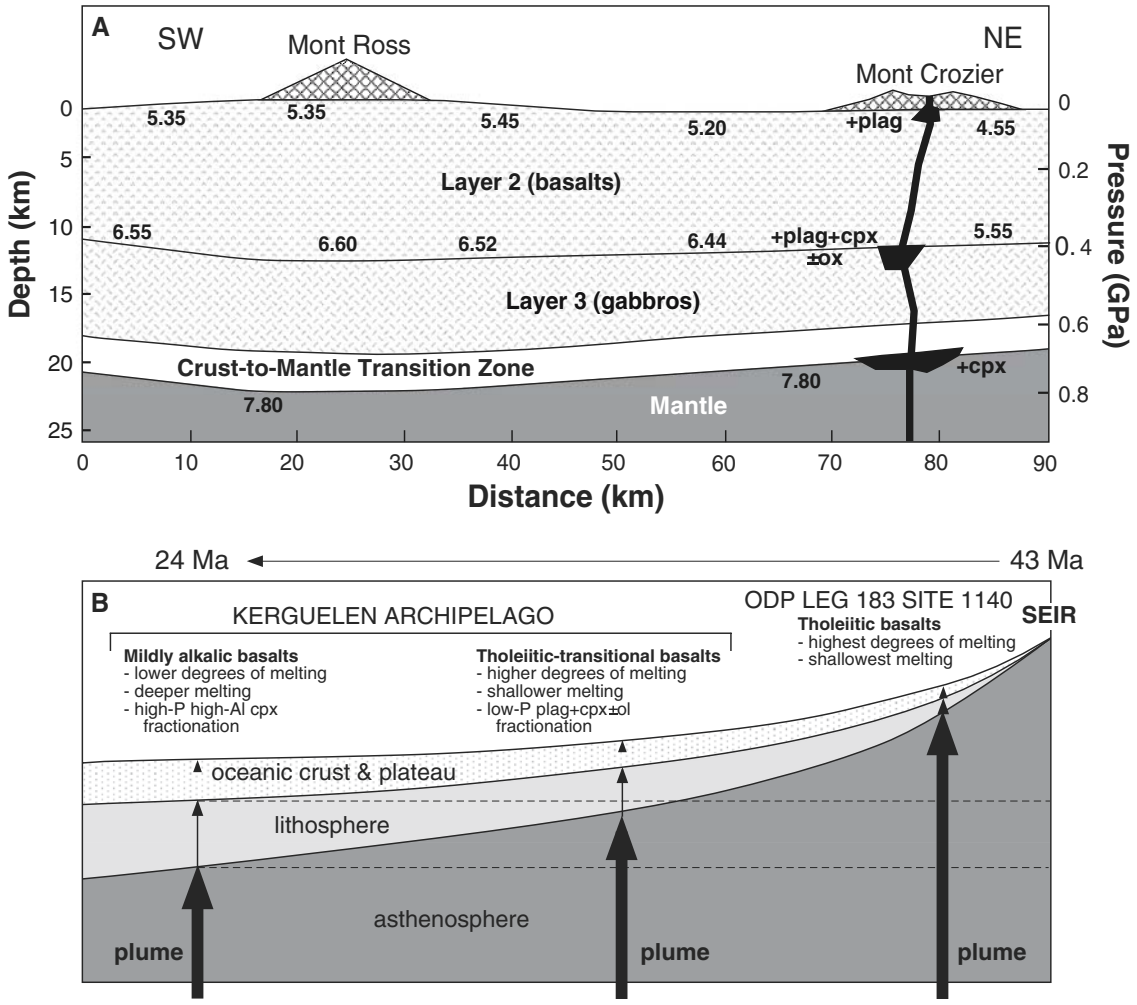

Fig. 7 **a** Schematic diagram showing the structure of the crust under the Kerguelen Archipelago based on the studies of Recq et al. (1994), Charvis et al. (1995), and Charvis and Operto (1999). The numbers in *bold* give the P-wave seismic velocities in km/s. Mont Ross is a <2 Ma trachybasaltic to trachytic stratovolcano constructed on the underlying flood basalts and Mont Crozier is a 978 m high summit on the Courbet Peninsula (see Fig. 1) underlain by 24–25 Ma mildly alkalic basalts. A simplified magmatic conduit system is shown from the Mont Crozier mildly alkalic lava sequence down through the crust and into the underlying mantle with the main fractionating phases indicated at the relevant depths based on results from this experimental study and the phenocryst compositional study of Damasceno et al. (2002). By 25 Ma, the crust had thickened through additions of gabbro and basalt such that the depth of the crust-mantle interface was within the field of stability for high-Al clinopyroxene. Ascending mildly alkalic basaltic magmas stalled and fractionated extensively in this region—high-Al clinopyroxene is likely a major component of the low-velocity crust-to-mantle transition zone. **b** Schematic diagram showing the variation in thickness of the crust and lithosphere beneath the Kerguelen Archipelago and Northern Kerguelen Plateau from 43 Ma when the Kerguelen mantle plume was centered on the Southeast Indian Ridge (SEIR) to 24 Ma, the time of eruption of the mildly alkalic basalts on the archipelago. The *thick black vertical arrows* indicate the relative position of the Kerguelen mantle plume at ~34 Ma (50 km from SEIR), 29 Ma (200 km from SEIR), and 24 Ma (400 km from SEIR); the thickness of the *arrows* is not scaled to the plume diameter. Impingement of the plume at the base of the lithosphere should occur at progressively deeper levels as the lithosphere cools; possible thermal erosion of the lithosphere by the hot mantle plume is not taken into account in this simplified hypothesis, nor is plate flexure due to an impinging plume (e.g., Mittelstaedt and Ito 2005). Deeper and lower extents of partial melting of the mantle after 25 Ma produce mildly alkalic basalts. Higher water contents in the mildly alkalic basalts compared to the older 26–29 Ma tholeiitic-transitional basalts on the archipelago stabilize clinopyroxene relative to plagioclase. The horizontal *dashed lines* are for reference only and show the asthenosphere-lithosphere and mantle-crust limits at 24 Ma for comparison with their thicknesses when the archipelago and plateau were closer to the ridge

~400 km (assuming opening rates of 35 mm/year; Royer and Sandwell 1989) as the Southeast Indian Ridge migrated to the northwest relative to the Kerguelen hotspot, likely through a series of small (<1 m.y.) jumps due to thermal weakening of the overlying plate surrounding the ridge axis (Small 1995). During this period, the chemistry of the erupted lavas changed from transitional-tholeiitic to mildly alkalic, and the contribution of the Southeast Indian Ridge depleted mantle component decreased to zero (Weis et al. 1998b, Frey et al. 2000a; Doucet et al. 2005). At the same time, the thickness of the crust and of the lithosphere would have progressively increased due to the continued addition of magmatic products to the crust (gabbros to seismic layer

3 and basalts to seismic layer 2) and to cooling of the lithosphere (Fig. 7b).

The consequence of thickening of the lithosphere was that the Kerguelen mantle plume was stalled at increasingly greater pressures and depths (Frey et al. 2000a), thus reducing the extent of decompression melting. This corresponds to the documented change from tholeiitic to tholeiitic-transitional to mildly alkalic basalts from 34 to 24 Ma. The Kerguelen mantle plume was able to ascend to much shallower levels when the plume and the ridge were relatively close (Fig. 7b), thus increasing the degree of melting and producing tholeiitic basalts. The 26–29 Ma tholeiitic-transitional basalts on the archipelago formed by melting at intermediate depths, ascended to higher structural levels than the 24–25 Ma mildly alkalic basalts due to the thinner crust, and were dominated by shallow-level fractionation of plagioclase + clinopyroxene ± olivine from relatively water-poor magmas. By 25 Ma, the base of the lithosphere had reached depths corresponding to the garnet-lherzolite stability field, which resulted in the production of mildly alkalic basaltic magmas from low extents of partial melting. As water behaves as an incompatible element during mantle melting (e.g., Michael 1995; Danyuschevsky et al. 2000), the mildly alkalic basalts would have had higher contents of dissolved water, thus enhancing the stability of clinopyroxene at the expense of plagioclase as shown in this study. Finally, by 25 Ma, the crust-mantle interface was sufficiently deep (15–20 km) that this region of potentially important density contrast became the site of extensive high-Al clinopyroxene fractionation and accumulation.

Conclusions

An experimental study on the role of clinopyroxene fractionation on major element trends and changes in alkalinity in tholeiitic to mildly alkalic basalts from the Kerguelen Archipelago demonstrates that high-Al clinopyroxene-dominated fractionation from a water-bearing (~1.2 wt.% H_2O), low MgO (~5 wt.%), transitional to mildly alkalic basalt (alkalinity index = 0.1) at elevated pressures (~0.9 GPa) produces geochemical trends similar to those observed in the relatively young 24–25 Ma mildly alkalic lavas present on the archipelago. High-Al clinopyroxene is likely an important component of the low-velocity crust-to-mantle transition zone at the base of the thick Northern Kerguelen Plateau (15–20 km depth). Elevated water contents in the mildly alkalic basalts stabilized clinopyroxene relative to plagioclase, which plays an important role in low-pressure fractionation during evolution of the older 26–29 Ma tholeiitic-transitional basalts in the northwestern parts of the archipelago, but not in the mildly alkalic basalts. Extensive clinopyroxene fractionation however does not result in significant changes in alkalinity of the residual melt compositions. The change from tholeiitic-transitional basaltic volcanism to mildly alkalic basaltic volcanism on the Kerguelen Archipelago at ~25 Ma appears to primarily reflect lower extents of melting, coupled with an increase in the depth of melting (garnet in the residue), within the Kerguelen plume source as previously proposed (Weis et al. 1998a; Frey et al. 2000a). This change in basalt chemistry is a function of the increasing thickness as the cooling lithosphere beneath the Northern Kerguelen Plateau as the distance from the Southeast Indian Ridge increased from 40 to 25 Ma, which forced decompression melting within the Kerguelen mantle plume to progressively deeper levels. Finally, the important role for high-pressure high-Al clinopyroxene fractionation in the mildly alkalic basalts reflects the increased water contents of the lower degree partial melts and stalling of the ascending magmas at the deepening crust-mantle interface, as the crust beneath the archipelago continued to thicken through addition of lower crustal gabbros and upper crustal basalts.

Acknowledgements We are very grateful to Michel Fialin for his assistance during microprobe work at the Université de Pierre et Marie Curie (Paris 6), and Hanna Nekvasil and Charles Mandeville for the FTIR analyses done at the American Museum of Natural History (New York). Discussions with and advice from Dimitri Damasceno were particularly useful during sample selection. Funding for this project was provided by the Communauté Française in Belgium (ARC Research Grant 98/03–233 to Weis and Scoates), the Center for High Pressure Research and the Dept. of Geosciences of the State University of New York at Stony Brook, NSF EAR9902931 to Lindsley, and NSERC Discovery Grants to Scoates and Weis. Many thanks to Tom Sisson and an anonymous reviewer for their useful comments on the manuscript and Tim Grove for editorial assistance.

References

Albarède F (1992) How deep do common basaltic magmas form and differentiate? J Geophys Res 97:10,997–11,009

Albarède F, Luais B, Fitton G, Semet M, Kaminski E, Upton BGJ, Bachèlery P, Cheminée J-L (1997) The geochemical regimes of Piton de la Fournaise volcano (Réunion) during the last 530,000 years. J Petrol 38:171–201

Andersen DJ, Lindsley DH, Davidson PM (1993) QUILF: a Pascal program to assess equilibria among Fe-Mg-Mn-Ti oxides, pyroxenes, olivine, and quartz. Comp Geosci 19:1333–1350

Baker MB, Stolper EM (1994) Determining the composition of high-pressure mantle melts using diamond aggregates. Geochim Cosmochim Acta 58:2811–2827

Bryan WB, Finger LW, Chayes F (1969) Estimating proportions in petrographic mixing equations by least square approximation. Science 163:926–927

Charvis P, Recq M, Operto S, Brefort D (1995) Deep structure of the northern Kerguelen Plateau and hotspot-related activity. Geophys J Int 122:899–924

Charvis P, Operto S (1999) Structure of the Cretaceous Kerguelen Volcanic Province (southern Indian Ocean) from wide-angle seismic data. Geodynamics 28:51–71

Chen C-Y, Frey FA (1983) Origin of Hawaiian tholeiite and alkalic basalt. Nature 302:785–789

Damasceno D (1996) Evolution magmatique de la série basaltique du Mont Crozier (Archipel de Kerguelen, océan Indien): étude pétrologique et chimique. Unpublished B.Sc. thesis, Université Libre de Bruxelles, Brussels, Belgium, p 47

Damasceno D, Nicolaysen K, Weis D, Scoates J, Frey FA, Yang HJ, Giret A (1997) The Kerguelen plume: constraints from the 24.5 Ma alkalic basalts at Mont Crozier (Kerguelen Archipelago). Fall AGU, San Francisco, CA, USA. EOS 78:F728

Damasceno D, Scoates JS, Weis D, Shimizu N, Frey FA, Wallace P (2000) Implications of trace element abundances in clinopyroxene phenocrysts and basaltic lavas from the Kerguelen Archipelago and Plateau. Spring AGU, Washington DC. EOS Trans, AGU 81:S340

Damasceno D, Scoates JS, Weis D, Frey FA, Giret A (2002) Mineral chemistry of mildly alkalic basalts from the 25 Ma Mont Crozier section, Kerguelen Archipelago: constraints on phenocryst crystallization environments. J Petrol 43:1389–1413

Damasceno de Oliveira D, Scoates JS, Weis D, Nicolaysen K, Frey FA, Giret A (1997) Phenocryst stratigraphy and geochemical variation in the Mount Crozier basaltic series, Kerguelen Archipelago: Implications for the crystallization history of plume-related magmatism. EUG 9, Strasbourg, France. Terra Nova 9:55

Danuschevsky LV, Eggins SM, Falloon TJ, Christie DM (2000) H_2O abundance in depleted to moderately enriched mid-ocean ridge magmas; Part 1: incompatible behaviour, implications for mantle storage, and origin of regional variations. J Petrol 41:1329–1364

Dixon JE, Stolper EM, Holloway JR (1995) An experimental study of water and carbon dioxide solubilities in mid-ocean ridge basaltic liquids. Part I: calibration and solubility models. J Petrol 36:1607–1631

Doucet SD, Weis D, Scoates JS, Nicolaysen K, Frey FA, Giret A (2002) The depleted mantle component in Kerguelen Archipelago basalts: petrogenesis of tholeiitic-transitional basalts from the Loranchet Peninsula. J Petrol 43:1341–1366

Doucet SD, Scoates JS, Weis D, Giret A (2005) Constraining the components of the Kerguelen mantle plume: a Hf-Pb-Sr-Nd isotopic study of picrites and high-MgO basalts from the Kerguelen Archipelago. Geochem Geophys Geosys: DOI 10.1029/2004GC000806

Freise M, Holtz F, Koepke J, Scoates J, Leyrit H (2003) Experimental constraints on the storage conditions of phonolites from the Kerguelen Archipelago. Contrib Mineral Petrol 145:659–672

Frey FA, Nicolaysen KA, Kubit BK, Weis D, Giret A (2002) Flood basalts from Mont Tourmente in the central Kerguelen Archipelago: the change from tholeiitic/transitional to alkali basalts at ~25 Ma. J Petrol 43:1367–1387

Frey FA, Weis D, Yang HJ, Nicolaysen K, Leyrit H, Giret A (2000a) Temporal geochemical trends in the Kerguelen archipelago basalts: evidence for decreasing magma supply from the Kerguelen plume. Chem Geol 164:61–80

Frey FA, Coffin MF, Wallace PJ, Weis D, Zhao X, Wise Jr SW, Wähnert V, Teagle DAH, Saccocia PJ, Reusch DN, Pringle MS, Nicolaysen KE, Neal CR, Müller RD, Moore CL, Mahoney JJ, Keszthelyi L, Inokuchi H, Duncan RA, Delius H, Damuth JE, Damasceno D, Coxall HK, Borre MK, Boehm F, Barling J, Arndt NT, Antretter (2000b) Origin and evolution of a submarine large igneous province: the Kerguelen Plateau and Broken Ridge, southern Indian Ocean. Earth Planet Sci Lett 176:73–89

Frey FA, Wise WS, Garcia MO, West H, Kwon ST, Kennedy A (1990) Evolution of Mauna Kea volcano, Hawaii: the transition from shield building to the alkalic cap stage. J Geophys Res 95:1271–1300

Furman T, Frey FA, Park K-H (1991) Chemical constraints on the petrogenesis of mildly alkaline lavas from Vestmannaeyjar, Iceland: the Eldfell (1973) and Surtsey (1963–1967) eruptions. Contrib Mineral Petrol 109:19–37

Geist DJ, McBirney AR, Duncan RA (1986) Geology and petrogenesis of lavas from San Cristobal Island, Galápagos Archipelago. Geol Soc Am Bull 97:555–566

Grégoire M, Cottin J-Y, Giret A, Mattielli N, Weis D (1998) The meta-igneous granulite xenoliths from Kerguelen Archipelago: evidence of a continent nucleation in an oceanic setting. Contrib Mineral Petrol 133:259–283

Grove TL, Bryan WB (1983) Fractionation of pyroxene-phyric MORB at low pressure: an experimental study. Contrib Mineral Petrol 84:293–309

Grove TL, Baker MB (1984) Phase equilibrium controls on the tholeiitic versus calc-alkaline differentiation trends. J Geophys Res 89:3253–3274

Hirschmann MM, Kogiso T, Maker MB, Stolper EM (2003) Alkalic magmas generated by partial melting of garnet pyroxenite. Geology 31:481–484

Hirschmann MM, Ghiorso MS, Wasylenki LE, Asimow PD, Stolper EM (1998a) Calculation of peridotite partial melting from thermodynamic models of minerals and melts. I. Review of methods and comparison of experiments. J Petrol 39:1091–1115

Hirschmann MM, Baker MB, Stolper EM (1998b) The effect of alkalis on the silica content of mantle-derived melts. Geochim Cosmochim Acta 62:883–902

Hoover JD, Irvine TN (1977) Liquidus relations and Mg-Fe partitioning on part of the system Mg_2SiO_4-Fe_2SiO_4-$CaMgSi_2O_6$-$CaFeSi_2O_6$-$KAlSi_3O_8$-SiO_2. Carn Inst Wash Yearbook 77:774–784

Ito G, Lin J, Graham, D (2003) Observational and theoretical studies of the dynamics of mantle plume–mid-ocean ridge interaction. Rev Geophys: DOI 10.1029/2002RG000117

Jang YD, Naslund HR, McBirney AR (2001) The differentiation trend of the Skaergaard intrusion and the timing of magnetite crystallization: iron enrichment revisited. Earth Planet Sci Lett 189:189–196

Keshav S, Gudfinnsson GH, Sen G, Fei Y (2004) High-pressure melting experiments on garnet clinopyroxenite and the alkalic to tholeiitic transition in ocean-island basalts. Earth Planet Sci Lett 223:365–379

Kushiro I (1996) Partial melting of fertile mantle peridotite at high pressures: an experimental study using aggregates of diamond. In: Basu A, Hart S (eds) Earth processes: reading the isotopic code. AGU Geophys Monogr 95:109–122

Lipman PW, Sisson TW, Ui T, Naka J (2000) In search of ancestral Kilauea volcano. Geology 28:1079–1082

Longhi J (2002) Some phase equilibrium systematics of lherzolite melting: I. Geochem Geophys Geosys: DOI 10.1029/2001GC000204

MacDonald GA, Katsura T (1964) Chemical composition of Hawaiian lavas. J Petrol 5:82–133

Mandeville CW, Webster JD, Rutherford MJ, Taylor BE, Timbal A, Faure K (2002) Determination of molar absorptivities for infrared absorption bands of H_2O in andesitic glass. Am Min 87:813–821

Mahoney J, Le Roex AP, Peng Z, Fisher RL, Natland JH (1992) Southwestern limits of Indian Ocean ridge mantle and the origin of low $^{206}Pb/^{204}Pb$ mid-ocean ridge basalt: isotope systematics of the central southwest Indian ridge (17°–50°E). J Geophys Res 97:19,771–19,790

Mahoney JJ, Jones WB, Frey FA, Salters VJM, Pyle DG, Davies HL (1995) Geochemical characteristics of lavas from Broken Ridge, the Naturaliste Plateau and southernmost Kerguelen Plateau: Cretaceous plateau volcanism in the southeast Indian Ocean. Chem Geol 120:315–345

Mattielli N, Weis D, Blichert-Toft J, Albarède F (2002) Hf isotopic evidence for a Miocene change in the Kerguelen mantle plume composition. J Petrol 43:1327–1339

McBirney AR, Williams H (1969) Geology and petrology of the Galápagos Islands. Geol Soc Am Mem 118:197

McBirney AR, Naslund HR (1990) The differentiation of the Skaergaard intrusion. Contrib Mineral Petrol 104:235–247

Michael PJ (1995) Regionally distinctive sources of depleted MORB: evidence from trace elements and H_2O. Earth Planet Sci Lett 131:301–320

Mittelstaedt E, Ito G (2005) Plume-ridge interaction, lithospheric stresses, and the origin of near-ridge volcanic lineaments. Geochem Geophys Geosys: DOI 10.1029/2004GC000860

Naumann TR, Geist D, Kurz M (2002) Petrology and geochemistry of Volcán Cerro Azul: petrologic diversity among the western Galápagos volcanoes. J Petrol 43:859–883

Naumann TR, Geist DJ (1999) Generation of alkalic basalt by crystal fractionation of tholeiitic basalt. Geology 27:423–426

Nekvasil H, Dondolini A, Horn J, Filiberto J, Long H, Lindsley DH (2004) The origin and evolution of silica-saturated alkalic suites: an experimental study. J Petrol 45:693–721

Newton RC, Charlu TV, Kleppa OJ (1974) Calorimetric investigation of stability of anhydrous magnesium cordierite with application to granulite facies metamorphism. Contrib Mineral Petrol 44:295–311

Nicolaysen K, Frey FA, Hodges KV, Weis D, Giret A (2000) $^{40}Ar/^{39}Ar$ geochronology of flood basalts from the Kerguelen Archipelago, southern Indian Ocean: implications for Cenozoic eruption rates of the Kerguelen plume. Earth Planet Sci Lett 174:313–328

Nougier J (1970) Contribution à l'étude géologique et géomorphologique des îles Kerguelen (Terres Australes et Antarctiques Françaises): Tomes I et II. Bulletin CNFRA, TAAF, Paris: 246, 440

Putirka K (1999) Clinopyroxene + liquid equilibria to 100 kbar and 2450 K. Contrib Mineral Petrol 135:151–163

Recq M, Le Roy I, Charvis P, Goslin J, Brefort D (1994) Structure profonde du mont Ross d'après la refraction sismique (îles Kerguelen, ocean Indien austral). Can J Earth Sci 31:1806–1821

Rhodes JM (1988) Geochemistry of the 1984 Mauna Loa eruption: implications for magma storage and supply. J Geophys Res 93:4453–4466

Rhodes JM (1996) Geochemical stratigraphy of lava flows sampled by the Hawaii Scientific Drilling Project. J Geophys Res 101:11,729–11,746

Royer J-Y, Sandwell DT (1989) Evolution of the eastern Indian Ocean since the late Cretaceous: constraints from Geosat altimetry. J Geophys Res 94:13,755–13,782

Sisson TW, Grove TL (1993) Experimental investigations of the role of H_2O in calc-alkaline differentiation and subduction zone magmatism. Contrib Mineral Petrol 113:143–166

Small C (1995) Observations of ridge-hotspot interactions in the Southern Ocean. J Geophys Res 100:17,931–17,946

Smith WHF, Sandwell DT (1997) Global sea floor topography from satellite altimetry and ship depth soundings. Science 277:1956–1962

Tikku AA, Cande SC (2000) On the fit of Broken Ridge and Kerguelen Plateau. Earth Planet Sci Lett 180:117–132

Toplis MJ, Carroll MR (1995) An experimental study of the influence of oxygen fugacity on Fe-Ti oxide stability, phase relations, and mineral-melt equilibria in ferro-basaltic systems. J Petrol 36:1137–1170

Wager LR (1960) The major element variation of the Layered Series of the Skaergaard intrusion and a re-estimation of the average composition of the hidden layered series and of the successive residual magma. J Petrol 1:364–398

Wallace P (2002) Volatiles in submarine basaltic glasses from the Northern Kerguelen Plateau (ODP Site 1140): implications for source region compositions, shallow magmatic processes, and plateau subsidence. J Petrol 43:1311–1326

Weis D, Frey FA (2002) Submarine basalts of the Northern Kerguelen Plateau: interaction between the Kerguelen plume and the Southeast Indian Ridge revealed at ODP site 1140. J Petrol 43:1287–1309

Weis D, Frey FA, Giret A, Cantagrel J-M (1998a) Geochemical characteristics of the youngest volcano (Mount Ross) in the Kerguelen Archipelago: inferences for magma flux, lithosphere assimilation and composition of the Kerguelen plume. J Petrol 39:973–994

Weis D, Damasceno D, Frey FA, Nicolaysen K, Giret A (1998b) Temporal isotopic variations in the Kerguelen plume: evidence from the Kerguelen Archipelago. Min Mag 62A:1643–1644

Weis D, Frey FA, Leyrit H, Gautier I (1993) Kerguelen archipelago revisited: geochemical and isotopic study of the Southeast Province lavas. Earth Planet Sci Lett 118:101–119

Weis D, Frey FA, Schlich R, Schaming M, Montigny R, Damasceno D, Mattielli N, Nicolaysen KE, Scoates JS (2002) Trace of the Kerguelen hot spot track: evidence from seamounts between the Kerguelen Archipelago and Heard Island, Indian Ocean. Geochem Geophys Geosys: DOI 10.1029/2001GC000251

Yang H-J, Frey FA, Weis D, Giret A, Pyle D, Michon G (1998) Petrogenesis of the flood basalts forming the northern Kerguelen Archipelago: implications for the Kerguelen plume. J Petrol 39:711–748